

Electronic Thesis and Dissertation Repository

4-30-2019 1:30 PM

Intraoperative Localization of Subthalamic Nucleus during Deep Brain Stimulation Surgery using Machine Learning Algorithms

Mahsa Khosravi, *The University of Western Ontario*

Supervisor: Patel, Rajni V., *The University of Western Ontario*

A thesis submitted in partial fulfillment of the requirements for the Master of Science degree in Electrical and Computer Engineering

© Mahsa Khosravi 2019

Follow this and additional works at: <https://ir.lib.uwo.ca/etd>



Part of the [Biomedical Commons](#), and the [Signal Processing Commons](#)

Recommended Citation

Khosravi, Mahsa, "Intraoperative Localization of Subthalamic Nucleus during Deep Brain Stimulation Surgery using Machine Learning Algorithms" (2019). *Electronic Thesis and Dissertation Repository*. 6163. <https://ir.lib.uwo.ca/etd/6163>

This Dissertation/Thesis is brought to you for free and open access by Scholarship@Western. It has been accepted for inclusion in Electronic Thesis and Dissertation Repository by an authorized administrator of Scholarship@Western. For more information, please contact wlsadmin@uwo.ca.

Abstract

This thesis presents a novel technique for localizing the Subthalamic Nucleus (STN) during Deep Brain Stimulation (DBS) surgery. DBS is an accepted treatment for individuals living with Parkinson's Disease (PD). This surgery involves unilateral or bilateral implantation of a permanent electrode inside the STN to deliver electrical current to neural tissue. The STN is a very small grey matter structure within the brain, which makes accurate placement a challenging task for the surgical team. Prior to placement of the permanent electrode, intraoperative microelectrode recordings (MERs) of neural activity are used to localize the STN. The placement of the permanent electrode and the success of the stimulation therapy depend on accurate localization. In this study, an objective approach was implemented to help the surgical team in localizing the STN. This is achieved by processing the MER signals and extracting features during the surgery to be used in a Machine Learning (ML) algorithm for defining the

electrophysiological borders of the STN. A new classification approach that can detect the dorsal borders of the STN during the operation is proposed. MER signals from 100 PD patients were recorded and used to validate the performance of the proposed method. The results show that by extracting wavelet transformation features from MER signals and using a deep neural network architecture, it is possible to detect the border of the STN with an accuracy of 92%. The proposed method can be implemented in real-time during the surgery to assist the surgical team with the goal of enhancing the accuracy and consistency of electrode placement in the STN while reducing the operation time.

Keywords: Deep Brain Stimulation, Intraoperative Localization of the STN, Machine Learning, Deep Neural Network, Subthalamic Nucleus, Parkinson's Disease.

Co-Authorship Statement

The research presented in this thesis has been conducted and written by Mahsa Khosravi under the supervision of Dr. Rajni V. Patel. Parts of the material in this thesis were published in peer-reviewed journal and conference papers, or are under review. The research published in each paper has been mainly conducted and written by the principal author. For the research reported in all of the papers, Dr. Patel was the project leader and supervisor, guiding and directing the study. He and Dr. S. F. Atashzar contributed to idea development, theoretical and experimental evaluations, and writing and revising the papers.

The material presented in Chapter 2 has been published as:

- Mahsa Khosravi, Seyed Farokh Atashzar, Greydon Gilmore, Mandar S. Jog, and Rajni V. Patel, in "Electrophysiological Signal Processing for Intraoperative Localization of Subthalamic Nucleus during Deep Brain Stimulation Surgery", *IEEE Global Conference on Signal and Information Processing (GlobalSIP)*, 2018 Nov, pp. 424-428, IEEE.

The material presented in Chapter 3 has been published as:

- Mahsa Khosravi, Seyed Farokh Atashzar, Greydon Gilmore, Mandar S. Jog, and Rajni V. Patel, in "Unsupervised Clustering of Micro-Electrophysiological Signals for localization of Subthalamic Nucleus during DBS Surgery", *9th International IEEE EMBS Conference on Neural Engineering (NER)*, 2019.

A version of the material presented in Chapter 4 is currently under review for publication:

- Mahsa Khosravi, Seyed Farokh Atashzar, Greydon Gilmore, Mandar S. Jog, and Rajni V. Patel," Intraoperative Localization of STN during DBS Surgery using a Data-driven Deep Neural Network Model", submitted to the *IEEE Journal of Biomedical and Health Informatics*, 2019.

To my beloved parents,
Tayeb and Mehri,
who have always encouraged me to learn and grow.

Acknowledgments

First and foremost, I would like to offer my sincere gratitude and appreciation to my supervisor, Dr. Rajni Patel, for his constant support, guidance, and motivation. He is one of the best teachers and mentors I have ever known and I would also like to thank him for being extremely caring and supportive. This project would not have been possible without his help, guidance and supervision. I would like to also thank Dr. Mandar Jog for his guidance and feedback on the medical aspects of this work. Special gratitude is also extended to Dr. Kermani, Dr. Shami, and Dr. Asokanthan for serving as my examination committee.

I would also like to thank my colleagues, lab mates and friends, Farokh and Greydon for their collaborations and efforts towards this study. A very special thanks to Greydon for taking the time to read through my thesis and provide me with immensely valuable comments.

I am endlessly thankful to all of my friends in London and CSTAR for all the joyful moments we shared.

This research was supported by the Natural Sciences and Engineering Research Council (NSERC) of Canada under the NSERC Discovery Grant RGPIN 1345; the AGEWELL Network of Centres of Excellence Grant AW CRP 2015-WP5.3, and the Canada Research Chairs Program.

Contents

Abstract	ii
Co-Authorship Statement	iv
Acknowledgments	vi
List of Figures	x
List of Tables	xiv
List of Acronyms	xv
1 Introduction	1
1.1 Introduction	1
1.1.1 Parkinson’s Disease: Symptoms and Etiology	1
1.1.2 Basal Ganglia, Dopamine and the Control of Movement	2
1.1.3 Pharmacological Treatments for Parkinson’s Disease	4
1.1.4 Neurosurgical treatments for PD: Deep Brain Stimulation	6
1.1.5 STN-DBS Surgical Procedure	8
Microelectrode Recordings (MER)	10
Challenges of Deep Brain Stimulation surgery	13
1.1.6 Application of Machine Learning for localization of STN- Literature Review	13
1.1.7 Thesis Objective	16
2 Supervised Classification Method for Locating Borders of STN	24
2.1 Introduction	24

2.2	Methods and Materials	26
2.2.1	Demographic Data and Data Acquisition	26
2.2.2	Feature Extraction: State-of-the-art Technique	27
2.2.3	Feature Extraction: short-time Fourier Transformation	31
2.3	Classifiers	32
2.3.1	Logistic Regression	32
2.3.2	Support Vector Machine	33
2.4	Results	35
2.5	Conclusion	36
3	Unsupervised Clustering Approach for Localization of STN	39
3.1	Introduction	39
3.2	Methods and Materials	41
3.2.1	Demographic Data	41
3.2.2	Surgical Procedure and Data Acquisition	42
3.2.3	Feature Extraction: short-time Fourier Transformation	42
3.2.4	Feature Extraction: Conventional Offline Features	45
3.3	Classifiers	46
3.3.1	K-means	47
3.3.2	Self Organized Map	47
3.3.3	Composite K-means-SOM	50
3.4	Results	50
3.5	Conclusion	51
4	Ensemble of Supervised Classifiers and Deep Neural Network Results on De-	
	tecting the STN	54
4.1	Introduction	54
4.2	Methods and Materials	57
4.2.1	Demographic Data and Data Acquisition	57
4.2.2	Feature Extraction	58
	Feature Extraction: Conventional Post-Operative Features	58

Feature Extraction: Fast Fourier Transformation	63
Feature Extraction: discrete Wavelet Transformation	63
4.3 Classifiers	65
4.3.1 The Ensemble of Multiple Classifiers	66
Weighted Majority Vote Rule	68
4.3.2 Deep Neural Networks	68
Deep Learning Parameters	69
4.4 Results	73
4.5 Conclusion	76
5 Concluding Remarks and Future Work	80
5.1 Concluding Remarks	80
5.1.1 Contributions	81
5.2 Future Directions	82
5.2.1 Collecting Intra-operative Data	82
5.2.2 Collecting Post-operative Data	82
5.2.3 Choosing the Best Channel	83
5.2.4 Localization of Globus Pallidus Pars interna (GPi)	83
5.2.5 Models and Hyperparameters	83
Curriculum Vitae	85
6 Curriculum Vitae	85

List of Figures

1.1	The basic anatomy of the brain showing the major regions within the basal ganglia area. Figure adapted from http://www.dana.org	3
1.2	Basal ganglia-thalamo-cortical circuit schematic in a healthy brain state. Neural signal transmission for movement control, begins at the SNc. The SNc projects the output to the striatum, which travels via direct and indirect pathways to the GPi/SNr. The GPi/SNr output signal projects to the thalamus, which directly communicates with the motor cortex.	4
1.3	Basal ganglia-thalamo-cortical circuit schematic in the PD brain. The thickness of the arrows describes the strength of the connection. Due to the degeneration of dopaminergic neurons in SNc, the signal transmission in both direct and indirect pathways are altered. The hyper-active STN signal is sent to the GPi, which leads to the increased inhibition of signals sent to the cortex.	5
1.4	This figure shows the implanted DBS electrode and its connection to the pulse generator.	7
1.5	Microelectrode trajectory reconstruction. The red lines indicate the depths that the neurosurgeon decided the microelectrodes are inside the STN. The reconstructions and visualizations were performed using custom Python codes, the Visualization Toolkit, and 3D Slicer v4.8 (https://www.slicer.org). T2-weighted 7T images were co-registered to the preoperative CT image containing the Leksell frame. Images were converted to the NIFTI file format using <code>dcm2niix</code> [30]. Co-registration was performed using rigid registration tools in <code>Niftyreg</code> [31]. The coordinates of the microelectrode trajectories were extracted from Stealthstation (Medtronic Corp, MN).	10

1.6	3D image of STN (right) with MER recordings (left) in a typical trajectory. (A) Upon entering the subthalamic nucleus, there is an increased compound firing rate and neural noise background, which decreases upon exiting the STN. (B) The typical DBS trajectory will traverse the thalamus (TH), followed by zona incerta (ZI), arriving at the subthalamic nucleus (STN), exiting into white matter (WM), and ending at the substantia nigra (SN) (Figure adapted from [32]).	11
1.7	MER trace from an anterior microelectrode trajectory from an STN-DBS case at University Hospital, London Health Sciences Center. The microelectrodes were advanced from 10.0 mm to 5.0 mm in 1.0 mm intervals. From 5.0 mm to the end of the trajectory, the unit was advanced in 0.5 mm increments. The green line indicates the dorsal border of the STN and the red line indicates the ventral border of the STN, as decided by the neurosurgeon.	12
1.8	Work flow diagram showing methods for data processing, feature extraction, and learning algorithms for STN localization.	17
2.1	(a) DBS electrode reconstruction, b) microelectrode trajectory reconstruction. T2-weighted preoperative MRI was co-registered to postoperative T1-weighted MRI. The images were brought into DARTEL (Diffeomorphic Anatomical Registration Through Exponentiated Lie) space using a non-linear registration. The images were then brought into MNI space, electrode positioning was estimated, and the 3D reconstruction was performed using the STN subdivision atlas by [12].	28
2.2	MER trace from an anterior microelectrode trajectory from a STN-DBS case at University Hospital. The microelectrodes advance from 10.0 mm to 5.0 mm in 1.0 mm intervals. From 5.0 mm to the end of the trajectory the unit is advanced in 0.5 mm increments. The green line indicates the dorsal border of the STN and the red line indicates the ventral border of the STN, as decided by the neurosurgeon.	29
2.3	Optimum hyper plane and support vectors for linearly separable data.	34

3.1	MER from an anterior electrode trajectory collected during an STN-DBS case. Negative depth values indicate above the nucleus and positive values indicate below. The green line indicates the dorsal border of STN and the red line indicates the ventral border of STN, as decided by the neurosurgical team. . . .	43
3.2	The figure shows power from the Short Time Fourier transform (STFT) in the frequency of 1000-3000Hz indicating a single-unit activity. The purple shaded area indicates where the nucleus was determined to be located based on the recordings. Red highlighted depth indicates which channel the surgeon decided to use. Each dotted line represents a recording depth. The power values are discrete and connected with a line for better representation. The negative depth values are above the nucleus and the positive values are below.	44
3.3	An example of the Best Unit Map or winning neurons for the sample data set with two clusters. Blue dots are the example data and red dots are the winning neurons which separated the dataset.	48
3.4	Hit Map units of the Self Organized Map with two neurons for STFT features. It shows the two clusters from the data. 3868 signals were labeled as zero and 1815 were labeled as class one.	49
4.1	Microelectrode trajectory reconstruction. The red lines indicate the depths that the neurosurgeon decided the microelectrodes are inside the STN. The reconstructions and visualizations were performed using custom Python codes, the Visualization Toolkit, and 3D Slicer v4.8 (https://www.slicer.org). T2-weighted 7T images were co-registered to the preoperative CT image containing the Leksell frame. Images were converted to the NIFTI file format using dcm2niix [13]. Co-registration was performed using rigid registration tools in Niftyreg [14]. The coordinates of the microelectrode trajectories were extracted from Stealthstation (Medtronic Corp, MN).	59

4.2	MER trace from an anterior microelectrode trajectory from an STN-DBS case at University Hospital, London Health Sciences Center. The microelectrodes were advanced from 10.0 mm to 5.0 mm in 1.0 mm intervals. From 5.0 mm to the end of the trajectory the unit was advanced in 0.5 mm increments. The green line indicates the dorsal border of the STN and the red line indicates the ventral border of the STN, as decided by the neurosurgeon.	60
4.3	The purple shaded area indicates where the nucleus was determined to be based on the recordings. The red highlighted depth indicates which channel the surgeon decided to use. Each dotted line represents a recording depth. Negative depth values are above the nucleus, and positive values are below. The black horizontal dashed line indicates the mean of zero crossing value in each trajectory.	62
4.4	Power from DFT in two distinct frequency bands. The upper figure shows the frequency of 500-1000Hz indicating multi-unit activity, and the other figure shows the frequency of 1000-3000Hz indicating single-unit activity. Negative depth values are above the nucleus, and positive values are below. The green line indicates the dorsal border of the STN and the red line indicates the ventral border of the STN, as decided by the neurosurgical team.	64
4.5	The discrete Haar mother Wavelet function.	65
4.6	A sample of fully connected feedforward neural network with one hidden layer.	69
4.7	Neural Network before and after dropout. (a) is a normal fully connected network. (b) is a network after the dropout. The crossed nodes have been dropped [21].	71
4.8	Relu, Tanh, and Sigmoid activation functions.	72
4.9	Accuracy of Classical Classifiers and Ensemble method for localizing STN. . .	75

List of Tables

2.1	Accuracy of Classifiers for Localizing STN	35
3.1	Accuracy of Unsupervised Clustering Algorithms	51
4.1	Confusion Matrix for the DNN Model	74
4.2	Accuracy of Deep Neural Network and Ensemble method	75

List of Abbreviations

DBS	Deep Brain Stimulation
DFT	Discrete Fourier Transformation
DNN	Deep Neural Network
DT	Decision Tree
DWT	Discrete Wavelet Transformation
GPI	Globus Pallidus internus
GPe	Globus Pallidus externus
KNN	<i>k</i> Nearest Neighborhood
LR	Logistic Regression
MER	Microelectrode Recording
NN	Neural Network
PD	Parkinson's disease
SNc	Substantia Nigra pars compacta
SNr	Substantia Nigra pars reticulate
SOM	Self Organized Map
STN	Subthalamic Nucleus
STFT	Short Time Fourier Transformation
SVM	Support Vector Machine

Chapter 1

Introduction

1.1 Introduction

1.1.1 Parkinson's Disease: Symptoms and Etiology

Parkinson's disease (PD) is a chronic and progressive neurological disease that affects 1% of people over 60 years of age [1, 2]. PD belongs to the movement disorder disease group, and it is 1.5 times more likely to present in the male population [3].

Most of the clinical motor features can be divided into hypokinesia and bradykinesia. Hypokinesia is the reduction in the frequency of regular movements such as arm swing, stride length, and blinking rate. Bradykinesia is the slowness of movements and fatigability of repetitive movements [4]. In the early stages of the disease, the most common motor symptoms are tremor, rigidity, bradykinesia, postural instability and shuffling of gait. Typically, tremor occurs during rest and involves the hands, legs, jaw, and lips [5]. Apart from these motor symptoms as the disease progresses nonmotor symptoms arise as well. Depression, dementia, and apathy are the most common neuropsychiatric comorbidities for individuals living with PD. Motor and nonmotor symptoms significantly affect the quality of life in individuals living with PD [3].

Motor features of PD result from the neurodegeneration of dopamine producing neurons in substantia nigra pars compacta (SNc) within the Basal Ganglia (BG). These neurons project their unmyelinated axons rostrally via the medial forebrain bundle to the striatum, where they

normally release dopamine [6]. Another pathophysiological sign of PD, although not present in every individual with PD, is the presence of Lewy bodies (aggregates of alpha-synuclein). While the exact cause of PD is unknown, genetic and environment factors could be among the causes [3].

1.1.2 Basal Ganglia, Dopamine and the Control of Movement

The BG is a group of subcortical nuclei within the brain, having a critical role in voluntary movement, control and cognitive behaviors [7]. The BG are on both sides of the brain, deep in cerebral the cortex, with no direct sensory inputs and no direct motor output to the spinal cord. As a result, the BG has no control over the specific movements of muscles directly. The BG indirectly controls movement mainly through the neurotransmitter dopamine, which plays a key role in the execution of desired movement [8].

The BG receives input signals from the cerebral cortex. Dopaminergic inputs in the SNc process and modulate this information and send the signal back to the cortex through the thalamus.

The BG has five major components which are (1) striatum, which is divided by the internal capsule into the caudate nucleus and putamen, it is also the largest component of the BG and has an important role in processing the inputs. (2) The globus pallidus (GP), which is divided into two segments by the medial medullary lamina; globus pallidus pars interna (GPi) and globus pallidus pars externa (GPe). (3) The substantia nigra (SN), which is also divided into the substantia nigra reticulata (SNr) and (SNc). (4) The final component of the BG is the subthalamic nucleus (STN), which is the structure that produces the largest amount of excitatory neurotransmitter glutamate [8]. Figure 1.1 shows the relative locations of these nuclei components inside the brain.

Most of the information processing in the BG happens within the striatum. In the striatum, most of the neurons in this part are of the medium spiny variety [9]. These neurons are responsible for receiving input from corticostriatal axons and releasing the neurotransmitter GABA. The neurons send projections through two important pathways named the direct pathway and the indirect pathways [9].

It is essential that both direct and indirect pathways of the BG be tightly balanced for vol-

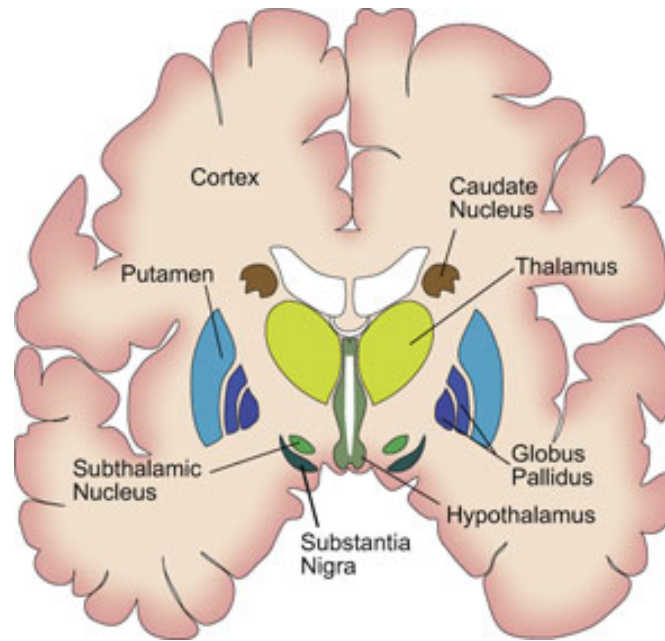


Figure 1.1: The basic anatomy of the brain showing the major regions within the basal ganglia area. Figure adapted from <http://www.dana.org>.

untary movement. If part of either pathway is impacted and unbalanced, a movement disorder may arise [10].

The direct pathway involves the striatum sending convergent inhibitory projections to the output nuclei. These neurons in the direct pathway have D1 dopamine receptors, which have direct pathways to the GPi, the output nucleus of the BG. The thalamus then sends widespread excitatory projections to the neocortex. These projections are vital for the initiation of movement; therefore, activation of the direct pathway stimulates movement.

Within the indirect pathway, the neurons contain D2 dopamine receptors and co-express the protein enkephalin. These cells project to the GPe and this in turn, inhibits neurons within the STN [11]. The indirect pathway neurons send signals to the output nuclei indirectly through the GPe and the STN. The activation of the indirect pathway acts to inhibit movement. Therefore, these two circuits have different effects on the output nuclei. Direct pathway stimulates and excited the output nucle while the indirect pathway inhibits the output from the striatum to the GPe [11, 12]. The output signal from the GPi is sent to the cortex through thalamus. The GPi and the SNr are the main outputs of the BG, and the STN transmit information from the striatum to the output of the BG [11].

Within the PD brain, there is a reduction in the number of SNc neurons that produce

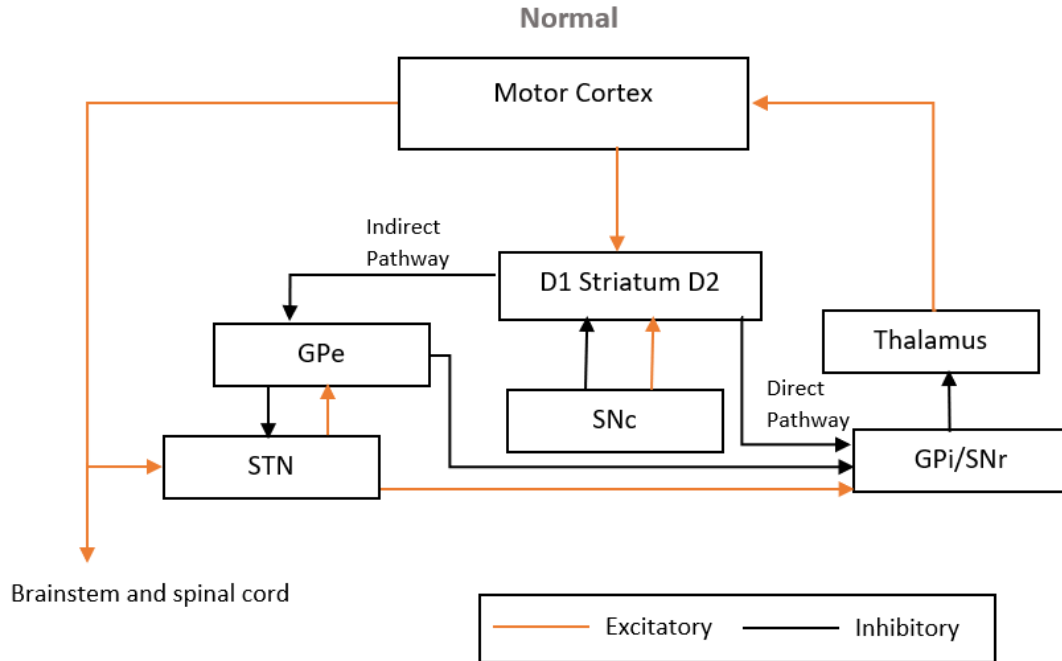


Figure 1.2: Basal ganglia-thalamo-cortical circuit schematic in a healthy brain state. Neural signal transmission for movement control, begins at the SNc. The SNc projects the output to the striatum, which travels via direct and indirect pathways to the GPi/SNr. The GPi/SNr output signal projects to the thalamus, which directly communicates with the motor cortex.

dopamine. Compared to a healthy brain, individuals living with PD have a dopamine deficiency, which reduces the activity of neurons in the direct pathway and over activates the neurons in the indirect pathway [13]. The imbalanced signal transmission in the direct and indirect pathway leads to PD symptoms. Figure 1.2 shows the BG neural circuit in a healthy brain state and Figure 1.3 shows the BG neural circuit in a PD brain.

It should be mentioned that the BG system is far more complex than what it is described here, and the pathophysiology of PD is not yet fully understood. However, this basic circuit model has helped clinicians find treatment options for PD.

1.1.3 Pharmacological Treatments for Parkinson's Disease

At the beginning stages of PD, the brain dynamically adapts to the dopamine depletion and by the time the cardinal symptoms of PD are present, patients have lost 80% of their striatal dopamine neurons and 50% of their SNc neurons [14]. Two main treatment options for individ-

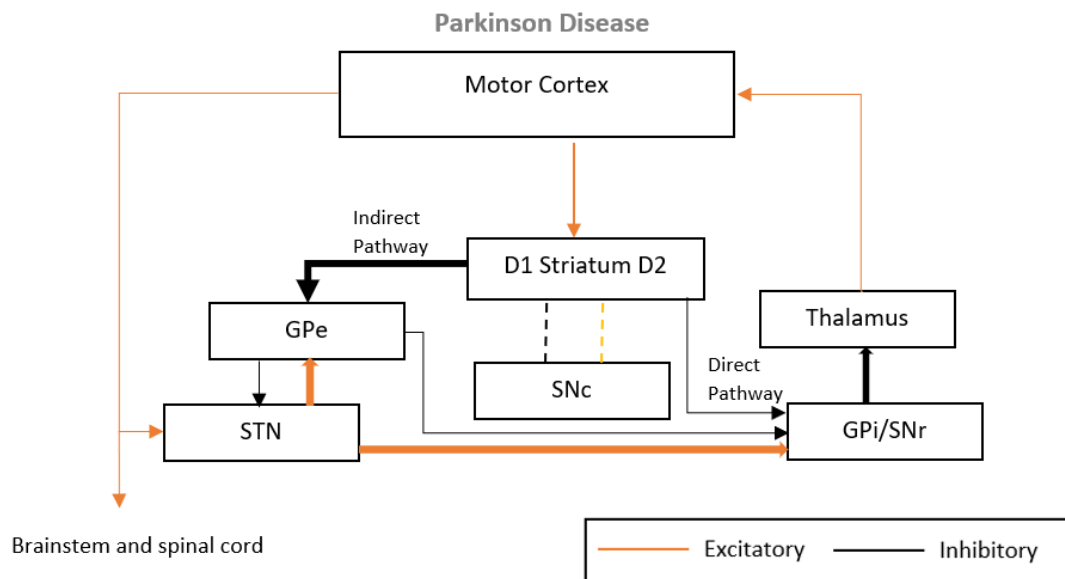


Figure 1.3: Basal ganglia-thalamo-cortical circuit schematic in the PD brain. The thickness of the arrows describes the strength of the connection. Due to the degeneration of dopaminergic neurons in SNc, the signal transmission in both direct and indirect pathways are altered. The hyper-active STN signal is sent to the GPi, which leads to the increased inhibition of signals sent to the cortex.

uals living with PD are pharmacotherapy and neurosurgery. Pharmacotherapy involves using oral medications and it usually precedes the surgical interventions for the beginning years of the disease [15].

Most PD patients show significant improvements initially with medical therapy, particularly, levodopa. Levodopa is a dopamine precursor, which can cross the blood-brain barrier, and is converted to dopamine in the brain. As a treatment for PD, levodopa restores the dopamine concentrations, which are reduced in the disease state [16, 17]. This works to alleviate the motor symptoms of PD such as rigidity, tremor and bradykinesia [17]. However, it can also cause some side effects for patients like nausea, abdominal discomfort, and vomiting; other medications may be taken to reduce these unpleasant side effects. Many patients experience increasing motor fluctuations and levodopa induced dyskinesias (LID) after a few years of using levodopa [5]. Levodopa is best started with a minimum dose (typically 50-100 mg/day) [18]. However, since PD is a progressive disease, the medication needs to be increased as the symptoms worsen. Although levodopa is the most effective medication to treat the motor symptoms of PD, it is not a cure for the disease [5, 16, 18].

For most patients, the response to levodopa progressively becomes more unpredictable with some severe side effects. These side effects have a significant impact on the quality of their life. Thus, for patients experiencing levodopa fluctuations, an alternative therapy, such as neurosurgical intervention, might be more beneficial [5, 16].

1.1.4 Neurosurgical treatments for PD: Deep Brain Stimulation

Deep brain stimulation (DBS) is a neurosurgical treatment for advanced PD and other kinds of movement disorders. This surgery is selected for patients who are responsive to levodopa, but suffer from severe fluctuations in the pharmacological response, despite optimal medical treatment [5, 16]. DBS can help to alleviate motor symptoms, such as tremor and can decrease bradykinesia, rigidity, and gait impairment [19, 20]. It also can reduce the amount of medications PD patients take on daily basis. This in turn helps to reduce the side effects patients may have been experiencing with the medications. During DBS surgery, a permanent electrode is implanted inside the brain to deliver high-frequency electrical pulses to either the STN or the internal segment of the GPi. These current pulses are most often monopolar at 130 Hz

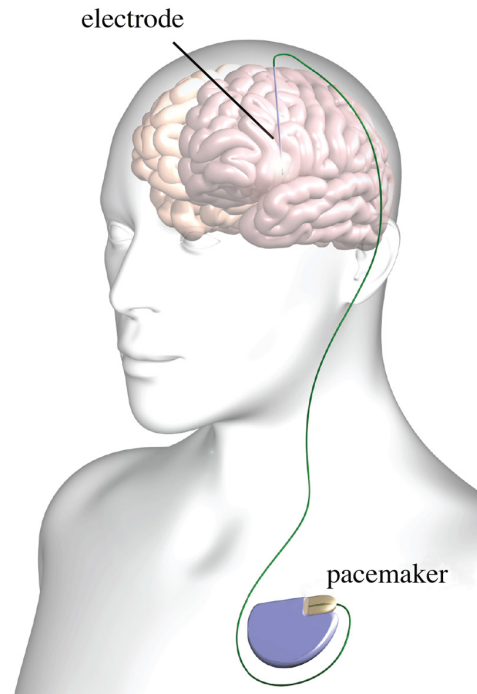


Figure 1.4: This figure shows the implanted DBS electrode and its connection to the pulse generator.

or 185 Hz, with a typical pulse width of $60 \mu\text{s}$ and a voltage around 3V. The electrodes are connected to a pulse generator that is located subcutaneously below the clavicle as shown in Figure 1.4 [19].

Electrical stimulation of the brain has been studied since 1870 to investigate brain function and the first report of cortical stimulation was published by Bartholow [21]. In 1987 Alim Benabid discovered that high-frequency stimulation of the brain had some clinical benefits for treatment of motor impairments [22]. These clinical benefits were like lesioning procedures used in the treatment of movement disorders previously [23]. However, DBS is now a more accepted treatment of movement disorders than lesioning procedures due to the reversibility of DBS. In addition, DBS allows the clinician to change the stimulation parameters such as voltage and frequency. Thus, DBS can be personalized for the optimal setting to each individual patient over time. Furthermore, DBS has minimal tissue damage in comparison to lesioning procedures and surgical ablation [23,24].

The reason for the efficacy of DBS surgery in the treatment of PD is still unknown. There is no complete theory regarding the mechanism of sending high-frequency electrical currents to

deep brain structures [25]. A popular theory, presented by Temel *et al.* [26], is that DBS reduces neuronal activities through a depolarization block, which will interrupt spontaneous activities within the neurons. Another hypothesis is that DBS can cause the activation of inhibitory afferents, which leads to the release of inhibitory neurotransmitters [26,27].

1.1.5 STN-DBS Surgical Procedure

The DBS surgery varies slightly between different health care centers, but it is often composed of two parts. The first part is the implantation of a small electrode inside the motor region of the STN, and the second part is to connect the electrode to a pulse generator under the collarbone of the patient. These two parts are usually done on separate days, the electrode is implanted first followed by the connect to the pulse generator through a thin wire under the skin. The first part, implanting the electrode usually takes about 6-8 hours of operation [25,26,28]. All patients withhold the short-acting Parkinson medications 12 hrs prior to the surgery.

The first step before electrode implantation in DBS surgery is the trajectory determination. The proper trajectory needs to be identified before the operation through medical images. A preoperative magnetic resonance imaging (MRI) sequence is obtained to determine the coordinates of the Anterior Commissure (AC), Posterior Commissure (PC) and the STN. An axial T2-weighted MRI image is usually used to identify the STN structure (Signa, 1.5T, General Electric, Milwaukee, Wis). The center of the STN is used as the surgical zero-point. Following stereotactic placement of the surgical Leksell frame on the patients' head (Elekta Instruments, Sweden), a stereotactic CT is obtained and fused with the preoperative MRI (StealthStation, Medtronic Corp, MN). The initial stereotactic STN coordinates are: 12.0 mm lateral, 2.0 mm posterior and 4.0 mm ventral to the midcommissural point (middle of AC and PC). Adjustments are then made according to the anatomy of the patient. The stereotactic head frame on the patient helps to guide the proper placement of the DBS electrodes [28].

The trajectory is determined before the surgery with respect to the anatomical landmarks AC and PC for the optimal placement of electrodes and reducing the risk of penetrating other parts of cerebral tissue. Although the MRI helps with estimating the location of the surgical target (STN), there may still be error that is introduced. The STN is a very small nucleus, located in the gray matter region of the brain. Furthermore, the optimal surgical target location

for STN stimulation differs between patients. Therefore, the MRI may not be accurate enough for locating the motor region of the STN. Thus, there is a need to record electrophysiological signals from the surgical target prior to DBS electrode implantation [28, 29].

The patient is brought to the operating room, a sterile field is established, and a burr hole is drilled anterior to the coronal suture. A computer-controlled microelectrode drive is mounted to the Leksell frame (StarDrive, FHC Inc., Bowdoinham, ME) to record electrophysiological signals. Some centers record through one track at a time, others investigate multiple tracks at once. In DBS surgeries that are performed at University Hospital, London, Ontario, up to five tracks are lowered down to record the activity of neurons toward the STN surgical target.

Five cannulas, with stylets, are lowered to 10.0 mm above the surgically planned target. The stylets are removed and replaced with five tungsten microelectrodes (60 μm diameter) with an impedance of 0.5-1.0 $m\Omega$ at 1kHz (FHC Inc., Bowdoinham, ME). Microelectrode signals are then captured from 10.0 mm to 5.0 mm above the target in 1.0 mm steps. From 5.0 mm onwards, a step size of 0.5 mm is used. The neurosurgical team projects and monitors the microelectrode recordings to find the borders of STN taking into account the fact that neuron activities inside the STN have asymmetrical spiking pattern at a high frequency with bursting patterns.

Once the ventral border of the STN is found, the recordings are completed (generally around 4.0 mm to 5.0 mm below the surgical target). When all the microelectrodes are implanted, a stimulation symptom review is done by the neurosurgeon on the patient. The goal of this is to identify the the most optimal target location for the final electrode implantation, which reduces the symptoms with fewest side effects. Tremor and rigidity are the most common symptoms that the neurosurgical team uses for optimal electrode positioning.

In the end, the neurosurgeon and electrophysiologist decide on the best microelectrode track; all microelectrodes are removed, and the final therapeutic electrode is introduced down the selected optimal trajectory. All the steps are repeated on the other side of the brain if the patient is receiving bilateral surgery. In Figure 1.5, an MRI of the trajectory of microelectrodes inside the brain is shown.

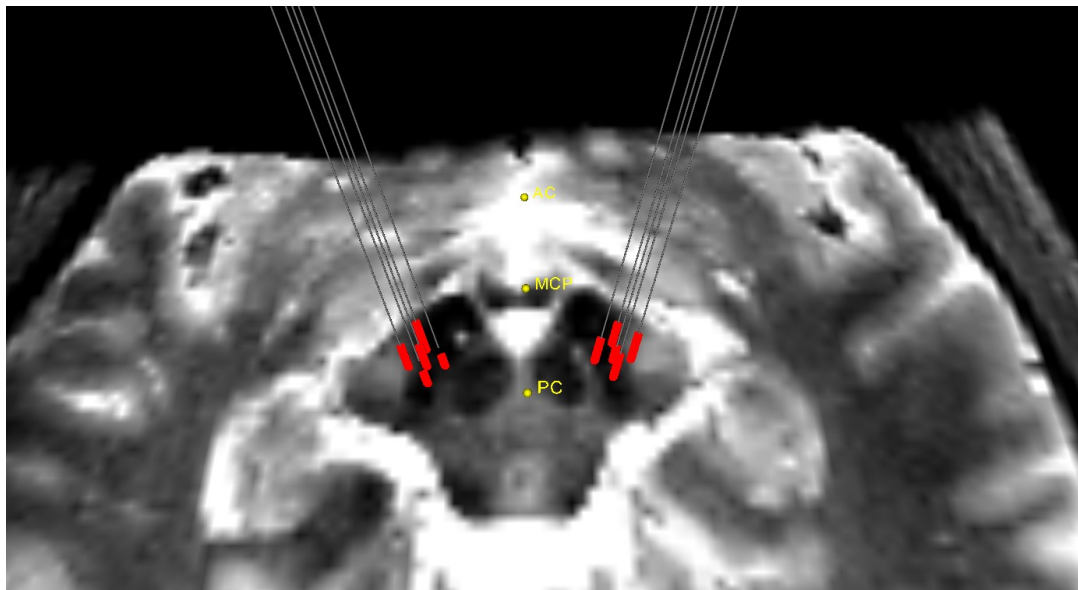


Figure 1.5: Microelectrode trajectory reconstruction. The red lines indicate the depths that the neurosurgeon decided the microelectrodes are inside the STN. The reconstructions and visualizations were performed using custom Python codes, the Visualization Toolkit, and 3D Slicer v4.8 (<https://www.slicer.org>). T2-weighted 7T images were co-registered to the pre-operative CT image containing the Leksell frame. Images were converted to the NIFTI file format using `dcm2niix` [30]. Co-registration was performed using rigid registration tools in Niftyreg [31]. The coordinates of the microelectrode trajectories were extracted from Stealthstation (Medtronic Corp, MN).

Microelectrode Recordings (MER)

In the brain, neurons transmit signals by generating electrical fields. Microelectrodes can record neural activity up to a radius of 200 microns. In DBS surgery, up to five microelectrodes are inserted. These microelectrodes are named based on their anatomical place; central, medial, lateral, anterior, and posterior [28].

Neural signal characteristics of each brain structure is different. The STN nucleus is identified by an abrupt increase in background neural activity and spiking rate. The spike patterns are also different in this nucleus as it is shown in the Figure 1.6. Therefore, recording the MER signals from different nuclei can assist the neurosurgeon to identify the STN target during the DBS surgery.

Also, a sample MER signal from a right-side anterior trajectory of the patient number 49 is shown in Figure 1.7. This figure demonstrates the difference in electrophysiological signal inside and outside the STN.

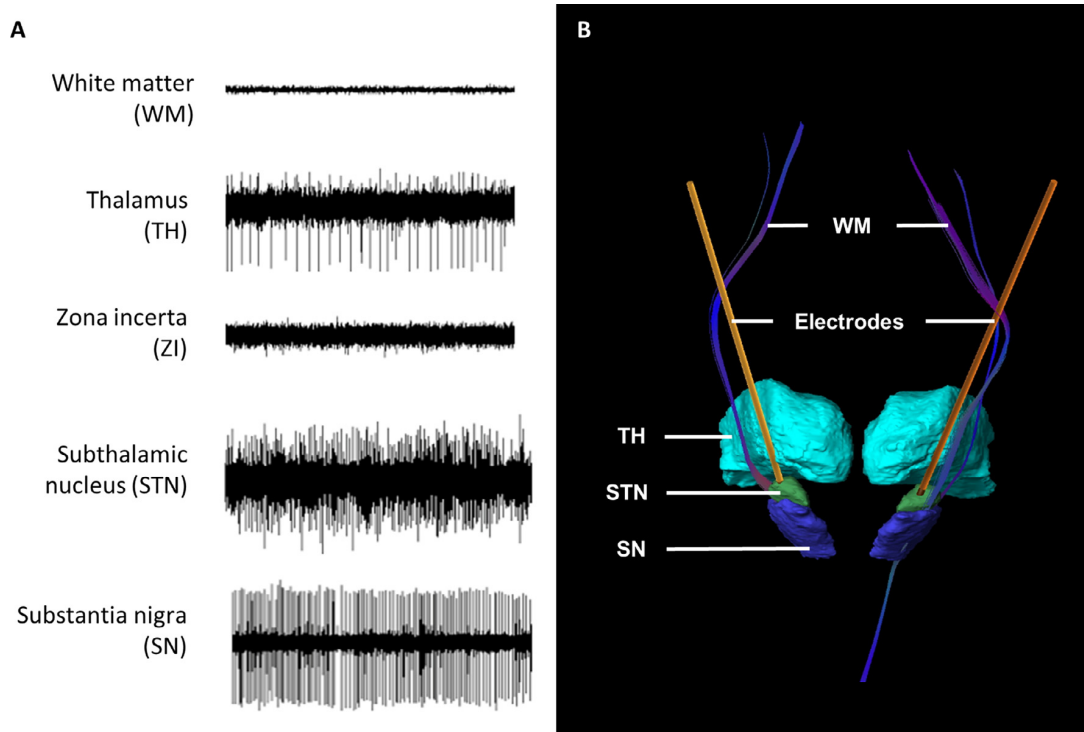


Figure 1.6: 3D image of STN (right) with MER recordings (left) in a typical trajectory. (A) Upon entering the subthalamic nucleus, there is an increased compound firing rate and neural noise background, which decreases upon exiting the STN. (B) The typical DBS trajectory will traverse the thalamus (TH), followed by zona incerta (ZI), arriving at the subthalamic nucleus (STN), exiting into white matter (WM), and ending at the substantia nigra (SN) (Figure adapted from [32]).

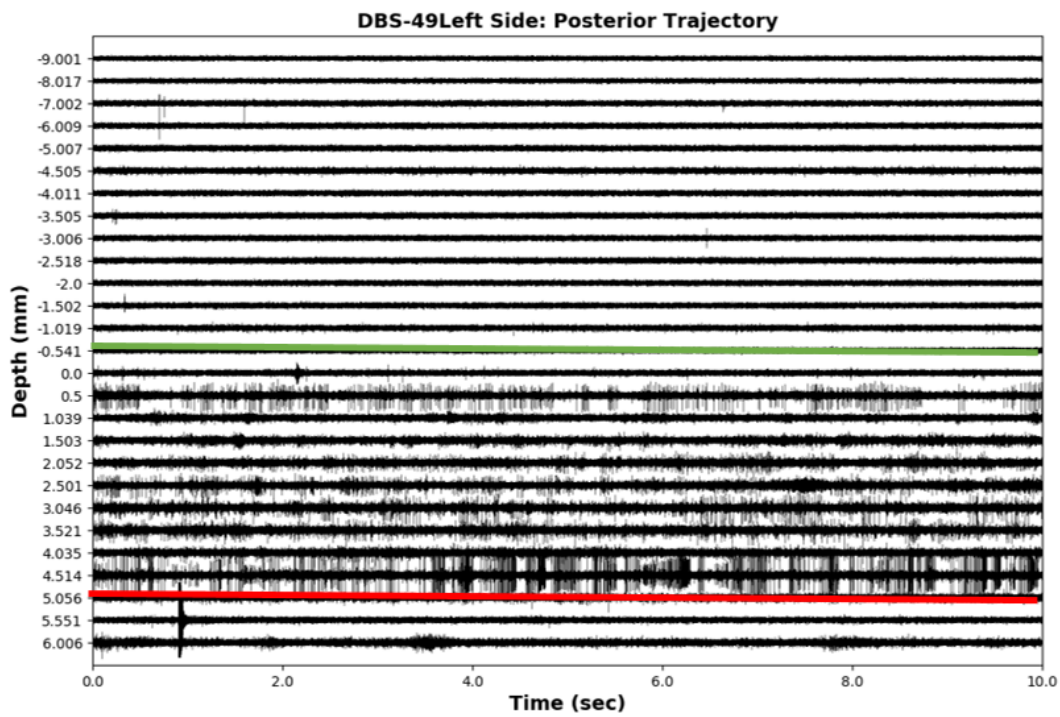


Figure 1.7: MER trace from an anterior microelectrode trajectory from an STN-DBS case at University Hospital, London Health Sciences Center. The microelectrodes were advanced from 10.0 mm to 5.0 mm in 1.0 mm intervals. From 5.0 mm to the end of the trajectory, the unit was advanced in 0.5 mm increments. The green line indicates the dorsal border of the STN and the red line indicates the ventral border of the STN, as decided by the neurosurgeon.

Challenges of Deep Brain Stimulation surgery

The outcome of DBS surgery is highly dependent on the accurate placement of the DBS electrode inside the STN. Since the STN is a very small (4-7mm) and it is in a deep anatomical region, precise and accurate implantation of the electrode is a difficult, challenging and time-consuming task. Accurate STN target localization also requires a high level of proficiency and expertise in the surgery. Due to the sensitivity and importance of implantation, significant intraoperative time is spent on localizing the borders of the STN. Sub-optimal positioning of DBS electrodes accounts for 40% of cases of inadequate efficacy of stimulation post operation [33].

In current practice, an MRI is used to locate the STN according to a visual atlas [34]. However, the exact location of the motor territory of the STN cannot be determined from MRI images [35]. Thus, intraoperative MERs can be used to localize the STN using electrophysiological properties of the brain tissue surrounding the STN and within the STN itself. In a typical DBS surgery, up to five microelectrodes are inserted through a burr hole in the skull. The microelectrodes record the electrophysiological activity along a track as they are sequentially advanced into the brain by the electrophysiologist [36]. Since each structure in the brain has its own characteristic neural activity (such as spike firing counts and patterns), the STN can be recognized over the background noise level. As a result, based on monitoring these electrophysiological activities, the neurosurgeon can decide when the microelectrode has entered the STN [34,37].

1.1.6 Application of Machine Learning for localization of STN- Literature Review

The topic of STN localization accuracy using electrophysiology has been studied in the literature, and several techniques have been implemented (e.g., [38–41]). An in-depth review has been published recently on all the studies conducted so far that used different feature extraction techniques and machine learning algorithms for localizing the STN nucleus [32]. In [32], Wan *et al.*, have provided a complete summary of the state-of-the-art algorithms that have achieved good accuracies. It was mentioned that most of the existing results are not robust enough for clinical implementation and further research is needed on the topic of detecting the STN nu-

cleus. Some major issues of localizing the STN during DBS surgery in the literature have been elaborated in [32]. One of the most important issues is the real-time implementation of localizing the STN. Postoperative processing steps are needed (such as some critical normalization) to prepare the feature space to be used for classification. These methods cannot be used intraoperatively [32].

In [39], multiple computational features have been suggested to identify the dorsal border of the STN using an unsupervised machine learning algorithm. This work was completed in 2015 [41] with the development of a new feature selection and normalization method that is based on the previously-suggested features. In [41], ten features were suggested as the best features to use in the classification problem. In addition, four classifiers were evaluated in [41]. Among the suggested algorithms, the Logistic Regression (LR) algorithm was reported as the most accurate scheme.

In [40], four features were selected from [39], and a Support Vector Machine (SVM) technique was used as the classifier. This work was continued in 2016 using a similar feature set from five PD patients and a neural network was used as the classification method [42].

Although high performance has been reported in some of the articles, the existing high performance techniques cannot be implemented in the operating room and *during* surgery. The reason is that the extracted features used in conventional techniques require post-operative processing steps (such as spike sorting and a specific normalization algorithm that requires information from the whole insertion trajectory) [39], [41].

However, the existing approaches can be used as post-operative validation techniques (which can help to evaluate the quality of the conducted operation after completion of the surgery). However, they do not allow for STN localization in an intraoperative manner. As a result, they cannot be used as a tool to provide feedback to the surgical team intraoperatively for enhancing the quality of concurrent surgery.

Moran *et al.* [43] have shown the feasibility of estimating entry and exit points of the STN based on normalized Root Mean Square (RMS) values. They have collected data from 27 PD patients and used Bayesian posterior probability to calculate the location of the electrode based on the normalized RMS values. In this study [43], Moran *et al.* have reported the error in predicting the STN entry and exit point, which is 0.30 ± 0.28 mm deviation from the

neurosurgeon's target result.

In [38], some visualization techniques of MER signals have been suggested to help identify the STN. In this study [38], Falkenberg *et al.* have used MER from 14 PD patients and have applied a few visualization methods such as Power Spectral Density (PSD), Marginal Probability Density function (mPDF) and Energy. It is reported that these visualization methods can improve patient outcome by helping neurosurgeons to identify target structures more accurately and quickly [38]. However, while this technique can be an assistive tool for the neurosurgeons, it is not feasible for use intraoperatively to automate the process.

In a preliminary study, based on data from five patients, Cardona *et al.* [44], evaluate the idea of using features without normalization and creating an online platform for STN localization. They suggest against normalization of features since the normalization process results in loss of high-frequency components of the signals, which can be informative in detecting the STN. However, they have reported that due to the challenging nature of locating the STN during DBS surgery, the accuracy of online techniques is significantly lower than offline techniques. It is mentioned in the paper that high accuracies are not guaranteed, and further analysis should be conducted on more data to enhance the accuracy of online systems [44].

In a recent paper [45], Valsky *et al.*, have used Normalized Root Mean Square (NRMS) and PSD to detect the ventral border of STN (the ending border) using an SVM and a Hidden Markov Model. In this paper, high accuracy is reported for the exit boundary of STN (0.04 ± 0.18 mm) on 131 microelectrode trajectory recordings. The proposed method in [45] requires NRMS which indicates that it is not feasible to implement intraoperatively for both entry and exit borders of STN.

To summarize, using the most advanced and most-recent techniques, the challenge of designing a data-driven model for detecting both the entry and exit borders of STN in an intraoperative manner is an unmet need. The existing problems are: (a) limited data to be used for generation of the model; (b) the need for using offline techniques and normalized features that require critical post-operative manipulation; and (c) limited machine learning power due to the use of classical techniques for the generation of the data-driven physiological model that can represent the borders of STN.

1.1.7 Thesis Objective

MER is used for identifying STN borders during DBS surgeries along with pre-planned trajectories. In current practice, the border detection of the STN nucleus is done manually by the neurosurgeon and electrophysiologist using the MERs. The accurate placement of the final electrode is critical for the optimal clinical outcome of this surgery. However, due to the small size of this nucleus, it is a highly challenging task for the surgical team. Furthermore, post-operative programming of the DBS device requires the neurologist's experience and time. Thus, an assistive tool for automating the localization of the STN target is an unmet need. The objective of this work is to develop an online algorithm for automating the process of detecting borders of the STN in DBS surgery.

For this purpose, the first step is to collect a rich and unique data-set to be used for evaluating the possibility of reaching high accuracy in the operating room. The second step is extracting features that can be calculated intraoperatively from MER signals with no requirement for postoperative normalization. Thus, the implementation of the proposed method can be feasible in the operative room during the DBS surgery. In the final step, different supervised and unsupervised machine learning algorithms are used to model the nonlinear neurophysiology to obtain the borders of the STN.

This study reports, for the first time, that using data-driven models, it is feasible to get an accuracy higher than 90% for localization of STN intraoperatively. All the methods implemented in this work had less than two seconds of execution time.

The structure of this thesis is as follows: In Chapter two, feature extraction methods are introduced, and two unsupervised machine learning algorithms are used for clustering MER signals without the neurosurgeon's labeling. In Chapter three, evaluation of multiple supervised classifiers is presented to locate the dorsal and ventral borders of the STN nucleus. Chapter four presents a new feature extraction method for better representation of microelectrode signals. An ensemble of four supervised classifiers and a deep neural network are implemented to automate the STN target localization process in DBS surgery. Chapter five provides concluding remarks for the thesis and includes a discussion of possible future directions and potential for the development of a supportive tool for assisting a neurosurgical team in order to achieve better outcomes for DBS surgery. A workflow of the study is shown in Figure 1.8.

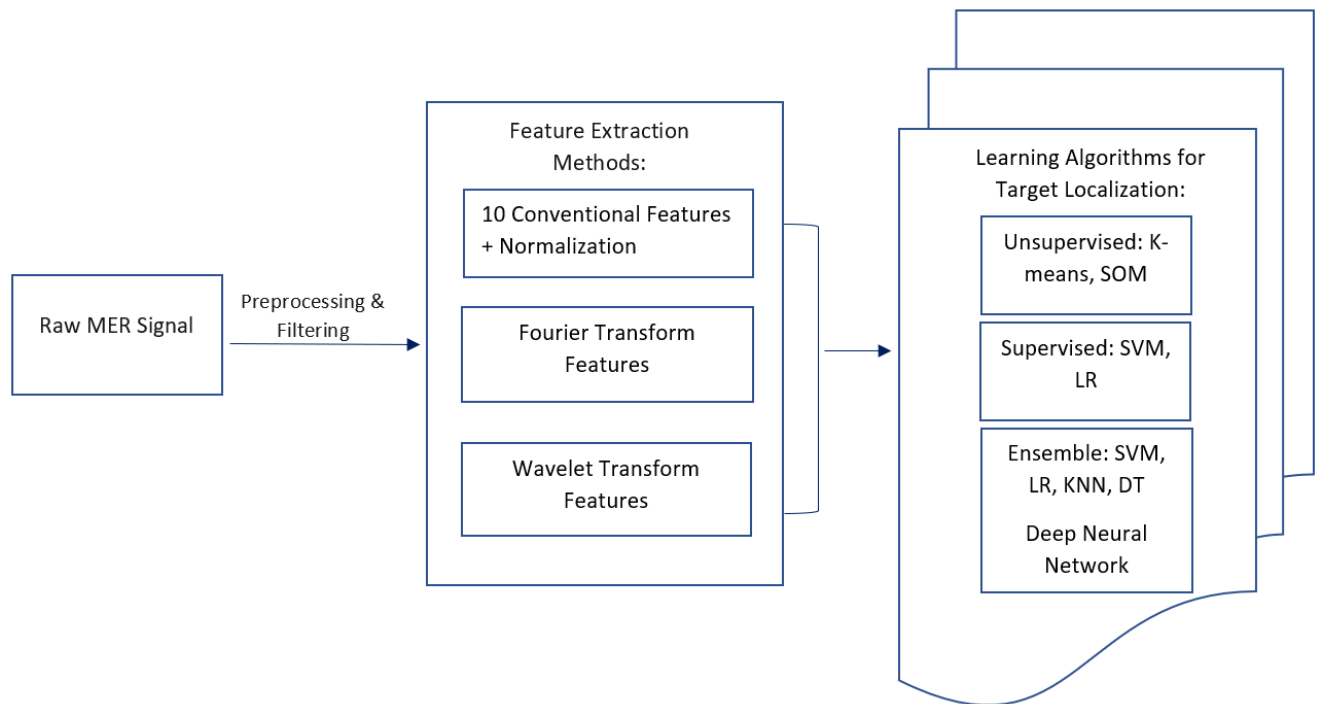


Figure 1.8: Work flow diagram showing methods for data processing, feature extraction, and learning algorithms for STN localization.

Bibliography

- [1] G. E. Alexander, “Biology of Parkinson’s disease: pathogenesis and pathophysiology of a multisystem neurodegenerative disorder,” *Dialogues in Clinical Neuroscience*, vol. 6, no. 3, p. 259, 2004.
- [2] D. G. Healy, M. Falchi, and e. a. O’Sullivan, “Phenotype, genotype, and worldwide genetic penetrance of LRRK2-associated Parkinson’s disease: a case-control study,” *The Lancet Neurology*, vol. 7, no. 7, pp. 583–590, 2008.
- [3] L. M. De Lau and M. M. Breteler, “Epidemiology of Parkinson’s disease,” *The Lancet Neurology*, vol. 5, no. 6, pp. 525–535, 2006.
- [4] A. Delval, P. Krystkowiak, J.-L. Blatt, E. Labyt, K. Dujardin, A. Destée, P. Derambure, and L. Defebvre, “Role of hypokinesia and bradykinesia in gait disturbances in Huntington’s disease,” *Journal of Neurology*, vol. 253, no. 1, pp. 73–80, 2006.
- [5] J. Jankovic, “Parkinsons disease: clinical features and diagnosis,” *Journal of Neurology, Neurosurgery & Psychiatry*, vol. 79, no. 4, pp. 368–376, 2008.
- [6] R. E. Burke and K. O’malley, “Axon degeneration in Parkinson’s disease,” *Experimental Neurology*, vol. 246, pp. 72–83, 2013.
- [7] R. L. Albin, A. B. Young, and J. B. Penney, “The functional anatomy of basal ganglia disorders,” *Trends in Neurosciences*, vol. 12, no. 10, pp. 366–375, 1989.
- [8] A. B. Nelson and A. C. Kreitzer, “Reassessing models of basal ganglia function and dysfunction,” *Annual Review of Neuroscience*, vol. 37, pp. 117–135, 2014.

- [9] L. R. Squire, “Declarative and nondeclarative memory: Multiple brain systems supporting learning and memory,” *Journal of Cognitive Neuroscience*, vol. 4, no. 3, pp. 232–243, 1992.
- [10] E. J. Brunenberg, P. Moeskops, and e. a. Backes, “Structural and resting state functional connectivity of the subthalamic nucleus: identification of motor stn parts and the hyper-direct pathway,” *PloS One*, vol. 7, no. 6, p. e39061, 2012.
- [11] M. R. DeLong, “Primate models of movement disorders of basal ganglia origin,” *Trends in Neurosciences*, vol. 13, no. 7, pp. 281–285, 1990.
- [12] S. Tekin and J. L. Cummings, “Frontal subcortical neuronal circuits and clinical neuropsychiatry: an update,” *Journal of Psychosomatic Research*, vol. 53, no. 2, pp. 647–654, 2002.
- [13] A. L. Bartels and K. L. Leenders, “Parkinson’s disease: the syndrome, the pathogenesis and pathophysiology,” *Cortex*, vol. 45, no. 8, pp. 915–921, 2009.
- [14] J. M. Fearnley and A. J. Lees, “Ageing and Parkinson’s disease: substantia nigra regional selectivity,” *Brain*, vol. 114, no. 5, pp. 2283–2301, 1991.
- [15] F. Tarazi, Z. Sahli, M. Wolny, and S. Mousa, “Emerging therapies for Parkinson’s disease: from bench to bedside,” *Pharmacology & therapeutics*, vol. 144, no. 2, pp. 123–133, 2014.
- [16] C. Curtze, J. G. Nutt, P. Carlson-Kuhta, M. Mancini, and F. B. Horak, “Levodopa is a double-edged sword for balance and gait in people with Parkinson’s disease,” *Movement Disorders*, vol. 30, no. 10, pp. 1361–1370, 2015.
- [17] Parkinson Study Group *et al.*, “Pramipexole vs levodopa as initial treatment for Parkinson’s disease: a randomized controlled trial,” *Jama*, vol. 284, no. 15, pp. 1931–1938, 2000.
- [18] R. Pahwa and K. E. Lyons, “Treatment of early Parkinson’s disease,” *Current Opinion in Neurology*, vol. 27, no. 4, pp. 442–449, 2014.

- [19] A. L. Benabid, "Deep brain stimulation for Parkinson's disease," *Current opinion in Neurobiology*, vol. 13, no. 6, pp. 696–706, 2003.
- [20] C. W. Olanow, M. F. Brin, and J. Obeso, "The role of deep brain stimulation as a surgical treatment for Parkinson's disease." *Neurology*, vol. 55, no. 12 Suppl 6, pp. S60–6, 2000.
- [21] R. Bartholow, "Art. i.—experimental investigations into the functions of the human brain." *The American Journal of the Medical Sciences (1827-1924)*, no. 134, p. 305, 1874.
- [22] A.-L. Benabid, P. Pollak, A. Louveau, S. Henry, and J. De Rougemont, "Combined (thalamotomy and stimulation) stereotactic surgery of the vim thalamic nucleus for bilateral Parkinson disease," *Stereotactic and functional Neurosurgery*, vol. 50, no. 1-6, pp. 344–346, 1987.
- [23] K. A. Follett, F. M. Weaver, and e. a. Stern, Matthew, "Pallidal versus subthalamic deep brain stimulation for Parkinson's disease," *New England Journal of Medicine*, vol. 362, no. 22, pp. 2077–2091, 2010.
- [24] C. Sidiropoulos, R. Walsh, C. Meaney, Y. Poon, M. Fallis, and E. Moro, "Low-frequency subthalamic nucleus deep brain stimulation for axial symptoms in advanced Parkinsons disease," *Journal of Neurology*, vol. 260, no. 9, pp. 2306–2311, 2013.
- [25] M. L. Kringelbach, N. Jenkinson, S. L. Owen, and T. Z. Aziz, "Translational principles of deep brain stimulation," *Nature Reviews Neuroscience*, vol. 8, no. 8, p. 623, 2007.
- [26] Y. Temel, A. Blokland, L. Ackermans, P. Boon, V. H. van Kranen-Mastenbroek, E. A. Beuls, G. H. Spincemaille, and V. Visser-Vandewalle, "Differential effects of subthalamic nucleus stimulation in advanced Parkinson disease on reaction time performance," *Experimental Brain Research*, vol. 169, no. 3, p. 389, 2006.
- [27] M. L. Janssen, A. A. Duits, A. M. Tourai, L. Ackermans, A. F. Leentjes, V. van Kranen-Mastenbroek, M. Oosterloo, V. Visser-Vandewalle, and Y. Temel, "Subthalamic nucleus high-frequency stimulation for advanced Parkinson's disease: motor and neuropsychological outcome after 10 years," *Stereotactic and functional Neurosurgery*, vol. 92, no. 6, pp. 381–387, 2014.

- [28] J. O. Dostrovsky and A. M. Lozano, "Mechanisms of deep brain stimulation," *Journal of the Movement Disorder Society*, vol. 17, no. S3, pp. S63–S68, 2002.
- [29] C. C. McIntyre, M. Savasta, L. Kerkerian-Le Goff, and J. L. Vitek, "Uncovering the mechanisms of action of deep brain stimulation: activation, inhibition, or both," *Clinical Neurophysiology*, vol. 115, no. 6, pp. 1239–1248, 2004.
- [30] X. Li, P. S. Morgan, J. Ashburner, J. Smith, and C. Rorden, "The first step for neuroimaging data analysis: Dicom to nifti conversion," *Journal of Neuroscience Methods*, vol. 264, pp. 47–56, 2016.
- [31] M. Modat, D. M. Cash, P. Daga, G. P. Winston, J. S. Duncan, and S. Ourselin, "Global image registration using a symmetric block-matching approach," *Journal of Medical Imaging*, vol. 1, no. 2, p. 024003, 2014.
- [32] K. R. Wan, T. Maszczyk, A. A. Q. See, J. Dauwels, and N. K. K. King, "A review on microelectrode recording selection of features for machine learning in deep brain stimulation surgery for Parkinson's disease," *Clinical Neurophysiology*, 2018.
- [33] M. S. Okun, M. Tagliati, M. Pourfar, H. H. Fernandez, R. L. Rodriguez, R. L. Alterman, and K. D. Foote, "Management of referred deep brain stimulation failures: a retrospective analysis from 2 movement disorders centers," *Archives of Neurology*, vol. 62, no. 8, pp. 1250–1255, 2005.
- [34] F. J. S. Castro, C. Pollo, O. Cuisenaire, J.-G. Villemure, and J.-P. Thiran, "Validation of experts versus atlas-based and automatic registration methods for subthalamic nucleus targeting on MRI," *International Journal of Computer Assisted Radiology and Surgery*, vol. 1, no. 1, pp. 5–12, 2006.
- [35] T. Foltynie, L. Zrinzo, and e. a. Martinez-Torres, Irene, "MRI-guided STN DBS in Parkinson's disease without microelectrode recording: efficacy and safety," *Journal of Neurology, Neurosurgery & Psychiatry*, p. 2010, 2010.

- [36] J. A. Saint-Cyr and A. Albanese, "STN DBS in PD selection criteria for surgery should include cognitive and psychiatric factors," *Neurology*, vol. 66, no. 12, pp. 1799–1800, 2006.
- [37] C. Pollo, F. Vingerhoets, E. Pralong, J. Ghika, P. Maeder, R. Meuli, J.-P. Thiran, and J.-G. Villemure, "Localization of electrodes in the subthalamic nucleus on magnetic resonance imaging," *Journal of Neurosurgery*, vol. 106, no. 1, pp. 36–44, 2007.
- [38] J. H. Falkenberg, J. McNames, J. Favre, and K. J. Burchiel, "Automatic analysis and visualization of microelectrode recording trajectories to the subthalamic nucleus: preliminary results," *Stereotactic and Functional Neurosurgery*, vol. 84, no. 1, pp. 35–45, 2006.
- [39] S. Wong, G. Baltuch, J. Jaggi, and S. Danish, "Functional localization and visualization of the subthalamic nucleus from microelectrode recordings acquired during DBS surgery with unsupervised machine learning," *Journal of Neural Engineering*, vol. 6, no. 2, p. 026006, 2009.
- [40] P. Guillen, F. Martinez-de Pison, R. Sanchez, M. Argaez, and L. Velazquez, "Characterization of subcortical structures during deep brain stimulation utilizing support vector machines," in *Engineering in Medicine and Biology Society (EMBC), IEEE*. IEEE, 2011, pp. 7949–7952.
- [41] V. Rajpurohit, S. F. Danish, E. L. Hargreaves, and S. Wong, "Optimizing computational feature sets for subthalamic nucleus localization in DBS surgery with feature selection," *Clinical Neurophysiology*, vol. 126, no. 5, pp. 975–982, 2015.
- [42] P. Guillén, "Deep learning applied to deep brain stimulation in Parkinsons disease," in *Latin American High Performance Computing Conference*. Springer, 2016, pp. 269–278.
- [43] A. Moran, I. Bar-Gad, H. Bergman, and Z. Israel, "Real-time refinement of subthalamic nucleus targeting using bayesian decision-making on the root mean square measure," *Movement disorders: official journal of the Movement Disorder Society*, vol. 21, no. 9, pp. 1425–1431, 2006.

-
- [44] H. D. V. Cardona, J. B. Padilla, R. Arango, H. Carmona, M. A. Alvarez, E. G. Estellés, and A. A. Orozco, “NEUROZONE: On-line recognition of brain structures in stereotactic surgery-application to Parkinson’s disease,” in *Engineering in Medicine and Biology Society (EMBC)*,. IEEE, 2012, pp. 2219–2222.
- [45] D. Valsky, O. Marmor-Levin, M. Deffains, R. Eitan, K. T. Blackwell, H. Bergman, and Z. Israel, “Stop! border ahead: A utomatic detection of subthalamic exit during deep brain stimulation surgery,” *Movement Disorders*, vol. 32, no. 1, pp. 70–79, 2017.

Chapter 2

Supervised Classification Method for Locating Borders of STN

2.1 Introduction

Parkinson's disease (PD) is the second most common neurodegenerative disorder [1]. PD is caused by deficiency of dopamine in substantia nigra pars compacta of the basal ganglia (BG). Motor symptomatology includes: tremor, rigidity, bradykinesia, and postured instability [2]. Deep brain stimulation (DBS) has been used in severe cases to alleviate these symptoms. The most common surgical target is the subthalamic nucleus (STN) of the BG.

DBS surgery involves permanent implantation of therapeutic electrodes that deliver electrical current to the motor region of the STN [3]. The motor region of the STN is a very small target and the surgical outcome depends highly on the accuracy of the therapeutic electrodes. Sub-optimal positioning of DBS electrodes accounts for 40% of cases of inadequate efficacy of stimulation post operation [4]. Localizing the borders of STN for accurate placement of electrodes is a challenging, time consuming and sensitive surgical task [5].

Preoperative Magnetic Resonance Imaging (MRI) is the most common modality which has been used to plan the insertion trajectory of the electrodes [6]. During the surgery, a surgical frame is attached to the patient's head and the neurosurgeon drills a burr hole in the skull to allow passage of the electrodes. Generally, five microelectrodes are inserted and lowered into the STN. The target is the center of the STN and is obtained using preoperative MRI.

The final stage, prior to implantation of the therapeutic electrode, involves selecting which microelectrode is positioned most optimally within the STN. Most centers do not have the technology required to capture intraoperative images and they rely on interpretation of the MERs. Disparate electro-physiological activities exist between different brain structures, which is utilized when interpreting the MER data [6, 7]. Currently, neurosurgeons monitor the raw neural spiking data to determine the microelectrodes that entered the STN and at which depth.

This study presents a novel intraoperative learning algorithm to assist the neurosurgeon in determining the optimal placement of electrodes. This has the potential to (a) save time during the surgery, and (b) enhance the accuracy of electrode placement which directly enhances the quality of treatment. Over the past few years, researchers have tried to find the signature of STN using MER signals. The most significant criteria of STN are the increase in spike firing rate and changes in the spike firing patterns [8]. State-of-the-art techniques have been reported in [9–11].

In this regard, [9] has suggested thirteen MER features to identify the dorsal border of the STN using an unsupervised machine learning algorithm. This work was completed in 2015 with the development of a new feature selection and normalization method that is based on the previously-suggested thirteen features [11]. In [11], ten out of the thirteen features were suggested as the best features to use in the classification problem. In addition, in the literature, four classifiers are evaluated in [11]; among them the Logistic Regression (LR) algorithm is reported as the most accurate scheme. In addition to the above, in [10], four features were selected from [9], and a Support Vector Machine (SVM) technique was used as the classifier. Although in [11] and [10], high accuracy was reported for classifying the STN based on a specific data set, the technique was not designed to be used in an intraoperative manner.

In this regard, it should be mentioned that for calculation of the features designed in [11], information about the whole insertion trajectory is required. Thus, the algorithm in [11] and [10] can be used as a postoperative validation method. However, it cannot guide the neurosurgeon during the DBS surgical procedure.

To address the above-mentioned issue, in this study we present a new method of feature selection using a short-time Fourier transform that can be extracted from the MER signals in an intraoperative manner. The Fourier transform has been widely used in the literature to

extract frequency features from brain signals.

To evaluate the performance of the proposed technique, in comparison to the most recent accurate existing methods in the literature (published in [11]) we have conducted a retrospective clinical study. In the study, we extracted MER signals for 20 patients with PD who had previously undergone the DBS procedure. The data was collected during DBS surgeries performed in University Hospital, London Health Sciences Center, London, ON, Canada. To conduct the comparison, the ten best features (which need to be calculated in a postoperative manner) proposed in [11] were calculated and used to implement the method proposed in [11] based on the LR algorithm.

The performance of the method proposed in this study is also evaluated based on the collected clinical data. The results of the comparative study support the effectiveness of the designed technique in comparison to the existing methods in the literature. It was shown that the method proposed in this study significantly improved the accuracy of STN localization while using MER features that can be collected during surgery intraoperatively. As a result, the proposed technique has the potential to be used in the operating room for assisting neurosurgeons, while reducing the operating time.

2.2 Methods and Materials

2.2.1 Demographic Data and Data Acquisition

In this part, we used MER signals from 20 PD patients who had previously undergone DBS implantation. The average age was 59 ± 8 yrs (13 male and 7 female). Most of the patients have 5 implanted microelectrodes bilaterally. The total number of implanted electrodes that were used in this study was 180. The study was approved by the Human Subject Research Ethics Board (HSREB) at the University of Western Ontario.

All patients discontinued short-acting Parkinson medications 12 hrs prior to the surgery. A preoperative MRI was obtained to determine the coordinates of the Anterior Commissure (AC), Posterior Commissure (PC) and the STN using an axial T2-weighted image (Signa, 1.5T, General Electric, Milwaukee, Wis). The center of the STN was used as the surgical zero-point. Following stereotactic placement of the surgical Leksell frame on the patients' head (Elekta

instruments, Sweden), a stereotactic CT was obtained and fused with the preoperative MRIs (StealthStation, Medtronic Corp, MN).

In the operating room, a burr hole was drilled just anterior to the coronal suture. The dura mater was opened and the pial surface was coagulated. The Leksell arc was attached to the head frame and set to the planned coordinates. The StarDrive (FHC Inc., Bowdoinham, ME) was mounted at 30.0 mm above the surgical target and 5 cannulas with stylets were lowered to 10.0 mm above the target. The stylets were then removed and five 60 μm diameter tungsten microelectrodes were inserted with an impedance of 0.5-1.0 $m\Omega$ at 1kHz (FHC Inc., Bowdoinham, ME).

Signals were recorded from 10.0 mm above the preoperatively determined target to well below the ventral border of the STN, generally looking for activity indicative of the substantia nigra (4.0 - 5.0 mm below the zero-point). The advancement of the microelectrode unit was performed with a computer-controlled motor drive (FHC Inc., Bowdoinham, ME). The microelectrodes were advanced in 1.0 mm increments from 10.0 mm to 5.0 mm above the target. From 5.0 mm to the end of the trajectory the microelectrodes were advanced in 0.5 mm increments. At each depth, advancement was paused to allow any drive or neural artifact to be resolved. In Figure 2.1, an MRI of electrode implantation and their trajectory toward the STN target is shown.

Once a clean recording was visualized a 10 second recording was collected prior to advancing the microelectrodes further. The signals were sampled (24kHz, 8-bit), amplified (gain: 10000) and digitally filtered (bandpass: 500-5000 Hz, notch: 60 Hz) with the Leadpoint recording station (Leadpoint 5, Medtronic). All the computational analyses were conducted in MATLAB. A sample MER signal from a right-side anterior trajectory is shown in Figure 2.2. This figure demonstrates the difference in electrophysiological signal inside and outside of the STN.

2.2.2 Feature Extraction: State-of-the-art Technique

To compare the performance of the technique proposed in this study with that of previous studies, we have extracted the most effective ten state-of-the-art features reported in [9], [11], and [10]. A list of these features for one 10-second interval is given below (the definitions are

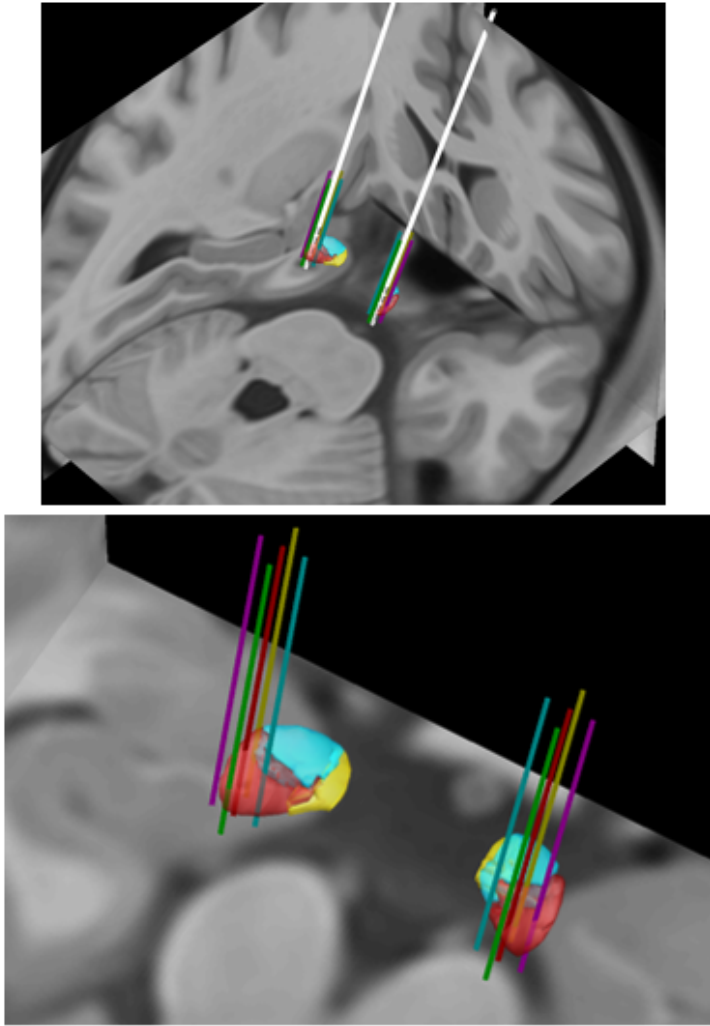


Figure 2.1: (a) DBS electrode reconstruction, b) microelectrode trajectory reconstruction. T2-weighted preoperative MRI was co-registered to postoperative T1-weighted MRI. The images were brought into DARTEL (Diffeomorphic Anatomical Registration Through Exponentiated Lie) space using a non-linear registration. The images were then brought into MNI space, electrode positioning was estimated, and the 3D reconstruction was performed using the STN subdivision atlas by [12].

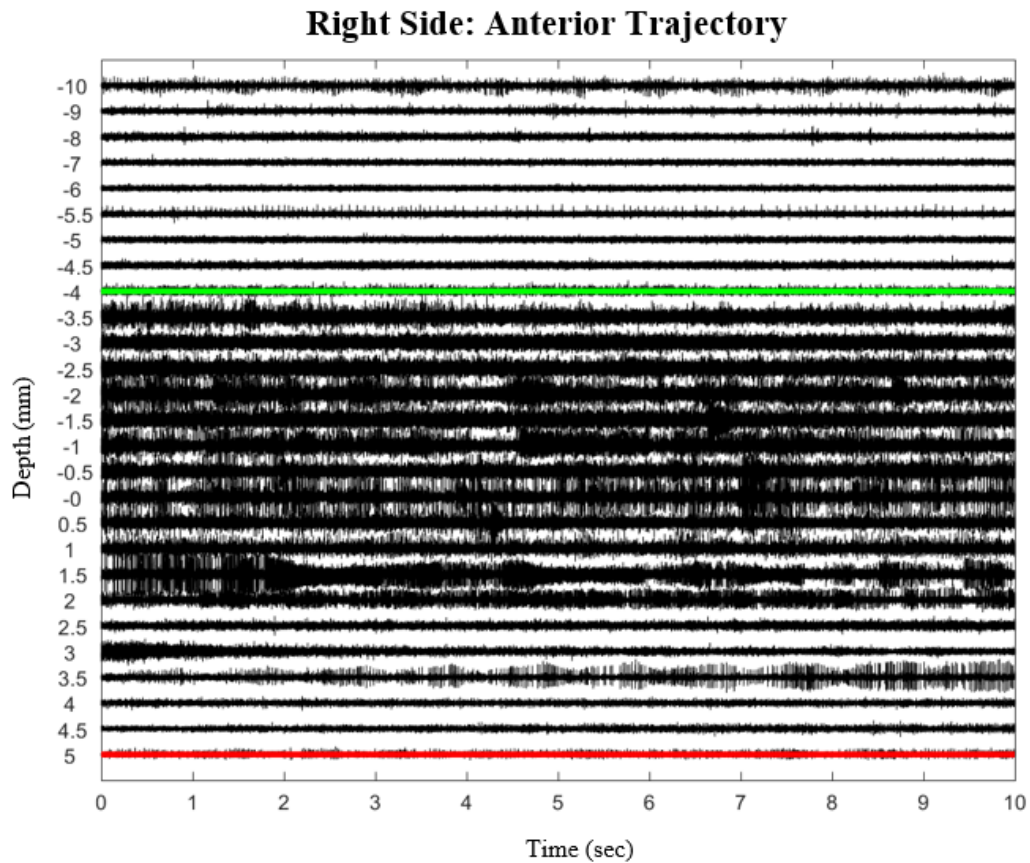


Figure 2.2: MER trace from an anterior microelectrode trajectory from a STN-DBS case at University Hospital. The microelectrodes advance from 10.0 mm to 5.0 mm in 1.0 mm intervals. From 5.0 mm to the end of the trajectory the unit is advanced in 0.5 mm increments. The green line indicates the dorsal border of the STN and the red line indicates the ventral border of the STN, as decided by the neurosurgeon.

taken from [10, 11]):

- 1) Number of spikes per the 10-second interval;
- 2) Standard deviation of time differences between the spikes of the 10-second interval;
- 3) Pause index: the ratio between the number of spikes greater than 50 ms to the number of spikes less than 50 ms;
- 4) Pause ratio: the ratio between the total time of inter spike intervals greater than 50ms to the total time of those less than 50ms;
- 5) Root Mean Square (RMS) value of the signal amplitude in the 10-second interval;

$$d = \sqrt{\frac{\sum_{i=1}^N x_i^2}{N}}; \quad (2.1)$$

where, each x_i corresponds to a sample in the dataset ($x_i \in X = \{x_1, x_2, \dots, x_n\}$) and N is the number of samples in each signal;

- 6) Spiking rate: number of spikes per unit time.
- 7) Teager Energy, which is used for estimating the instantaneous frequency of a signal and can be calculated as follows:

$$E = \sum_{i=2}^{N-1} x_i^2 - x_{i-1}x_{i+1}; \quad (2.2)$$

- 8) Zero crossing: the number of zero crossings in each 10-second interval:

$$k = \frac{1}{2} \sum_{i=1}^{N-1} |sgn(x_{i+1}) - sgn(x_i)|; \quad (2.3)$$

where, the function $sgn(x)$ returns 1 for $x > 0$, -1 for $x < 0$, and 0 for $x = 0$.

- 9) Curve length: the sum of consecutive distances between points in the 10-second interval

$$L = \sum_{i=1}^{N-1} |x_{i+1} - x_i| \quad (2.4)$$

10) Threshold (γ):

$$\gamma = \frac{3}{N-1} \sqrt{\sum_{i=1}^N (x_i - \bar{X})} \quad (2.5)$$

where \bar{X} is the average of the 10(s) time interval.

It is important to note that the technique proposed in [9] and the improved version of it reported in [11], require a specifically-designed normalization and standardization process before classification. This is due to the possibility of instability in feature calculation (very small denominator) resulting in significant errors in classification. Because these features may have different dynamic ranges, we might have some extremely large or extremely low values in the calculated features in one signal. Feature normalization is thus required to approximately equalize the ranges of the features so that they have approximately the same effect in the computation of similarity. However, it is not possible to conduct the needed normalization steps, used in [9] and [11] during the surgery. This makes the techniques proposed in [9] and [11] as approaches which can be used for postoperative assessment. As suggested in [11], the above-mentioned features are subtracted by the mean and divided by standard deviation of features in one trajectory. Thus, this method requires the MER data from one trajectory prior to implantation, which is not feasible intraoperatively.

2.2.3 Feature Extraction: short-time Fourier Transformation

Feature extraction can be form of dimensional reduction of signal processing which is tightly connected with pattern recognition process. One of the frequency analysis methods for extracting features from the signals is the discrete Fourier Transformation (DFT). The frequency features can be highly informative in this problem since the frequency content of neural activities in each structure is different. Thus, these features can highlight the differences between signals from inside the STN versus those from outside.

DFT has been widely used to extract features from biomedical stationary signals; short-time Fourier Transform (STFT) has been used for non-stationary signals. Many biomedical signals like microelectrode recordings from neurons are not constant over time and have abrupt changes through their period. Therefore, in this study, we have used STFT. The STFT introduced by Gabor applies the DFT on a fixed-size time window [13]; this way both time and

frequency components of the signals are retained in the extracted feature space. Mathematically for a signal $x(n)$, the STFT is given by:

$$STFT[x(n)](m, k) \Rightarrow X(m, k) = \sum_n h(n - m)x(n)e^{j2\pi nk/N} \quad (2.6)$$

where k is the frequency sample parameter, h is the analysis window function, and N is the total number of frequency samples. In this study we have used a window size of 0.02 ms for the STFT algorithm which gave us 1000 frequency features in the time period of the signal.

When the microelectrode is within the STN, there is a shift in the frequency domain of the MER signal. Thus, the STFT coefficients can provide valuable information about when the microelectrode enters the STN. Importantly, there is no need to normalize STFT coefficients, so these features can be extracted in an intraoperative manner from the MER signals during the operation. Also, there is no concern regarding stability.

2.3 Classifiers

After extracting features from MER signals, two classifiers, Logistic Regression and Support Vector Machines were applied to the signals. Each of these signals was labeled as zero or one. Label zero indicates that the electrode was outside of the STN and label one means that electrode was inside the STN. These labels were determined by the neurosurgeon and the electrophysiologist during the surgical procedure. Both of these specialists has performed more than 200 DBS surgeries.

2.3.1 Logistic Regression

Logistic Regression (LR) has been widely used in statistical analysis and this classifier is especially useful for problems with continuous features and discrete target outputs. The LR model

calculates the class membership probability in the data set [14] as shown below.

$$P(1|x, \theta) = \frac{1}{1 + e^{-\theta x}} \quad (2.7)$$

$$P(0|x, \theta) = 1 - P(1|x, \theta)$$

In (4.6), P is the probability of the class, x is the sample signal and θ is determined based on the dataset, usually by maximum-likelihood estimation.

2.3.2 Support Vector Machine

The Support Vector Machine (SVM) separates boundaries of data sets by solving an optimization problem. Depending on the kernel function of SVM, this separation can be linear or nonlinear with different degrees of nonlinearity and flexibility [15, 16]. Due to the complexity and nonlinearity of our data set; different kernel functions were used. In this study, we have tried different kernels including Linear, Quadratic and Cubic polynomials to separate our two classes. Kernel functions can map the original dimension of the data to a higher dimension, so that the SVM algorithm can find the hyperplane to separate the classes.

Let $x_i \in R, i = 0, 1, \dots, N$ (N is size of the training set) be the input vector and $y_i \in 0, 1$ be the corresponding labels. Label zero indicates the signals were outside the STN and label one corresponds to signals inside the STN.

$$y(x) = \text{sign}\left(\sum_{i=1}^N \alpha_i y_i \phi(x, x_i) + b\right) \quad (2.8)$$

where α_i are positive real constants and b is a real constant. $\phi(x, x_i)$ indicates the kernel of the classifier which can be linear: $\phi(x, x_i) = x_i^T x$ or polynomial: $\phi(x, x_i) = (x_i^T x + 1)^d$ in which d indicates the degree of the polynomial. The $\text{sign}(x)$ function returns 1 for $x > 0$, -1 for $x < 0$, and 0 for $x = 0$. In Quadratic and Cubic kernels, d is equal to two and three respectively. A sample of the optimum hyper plane which provides the maximum margin between classes is shown in Figure 2.3.

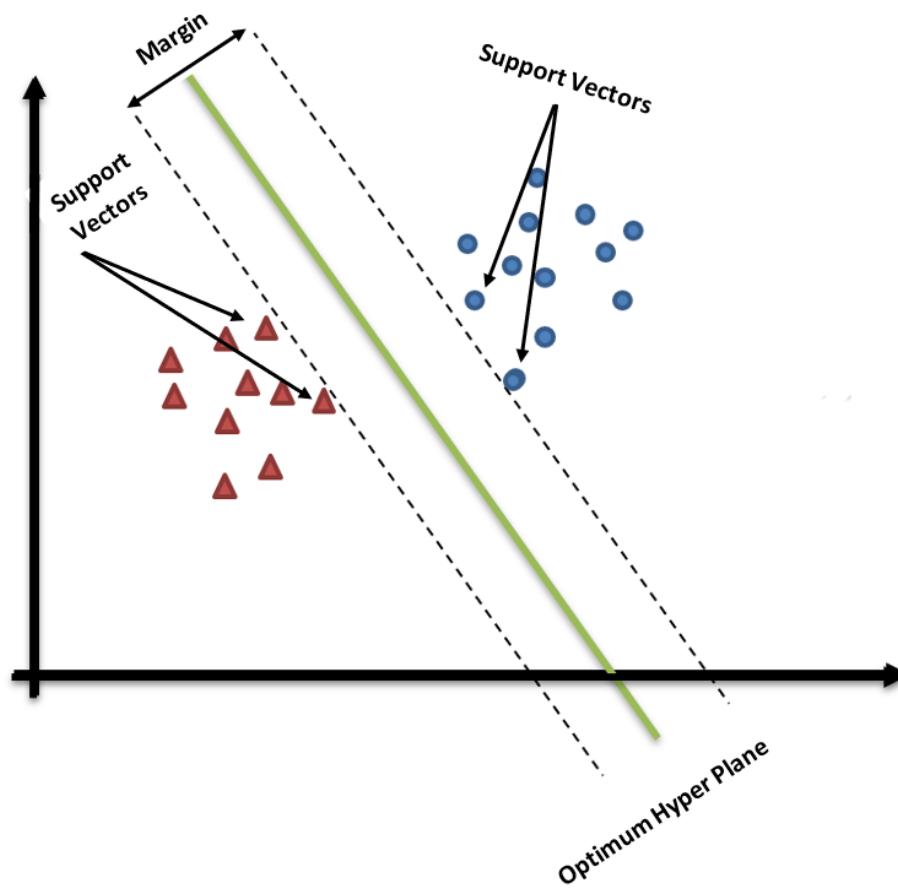


Figure 2.3: Optimum hyper plane and support vectors for linearly separable data.

2.4 Results

As mentioned in section 2.2.1, each signal was a 10 second recording from a specific depth. On average we had signals for 25 depths for each electrode. Furthermore, an average of ten microelectrodes were used for each patient. This study used MER data from 20 patients who had undergone DBS surgery previously. Most of the patients had bilateral DBS, while only a few had unilateral. The total number of samples was 3986. We extracted the ten features explained in Section 4.2.2 in addition to the STFT coefficients from the electrophysiological signals. Table (3.1) contains the results of ten-fold cross validation. The ten-fold cross validation method divides the training set into ten equally sized sections randomly. It takes out one section for validation or testing the classifier and uses the other nine sections for training. The same method is repeated ten times on the input data and the accuracy is calculated each time. At the end, the final accuracy of the classifier is equal to the average of ten accuracy result from the ten folds of the data set.

As can be seen, the highest accuracy has been achieved using STFT features and the SVM classifier with a Cubic kernel. As a result, we proposed this combination for detection of STN during DBS surgeries. Based on the achieved results, we can conclude that STFT features may be more informative than conventional features used in the literature.

This might be due to the capability of STFT features in highlighting the differences in spike activities in the frequency domain. Also, as mentioned above, unlike conventional techniques, using STFT, (a) there is no concern of instability in feature calculation, and (b) there is no need for post-normalization of the features; thus, the features can be calculated during the surgery and this makes it possible to help the neurosurgeon during the DBS procedure. In addition, based on the results, SVM with the Cubic kernel function is recommended as a nonlinear classifier with acceptable computational cost.

Table 2.1: Accuracy of Classifiers for Localizing STN

Features\classifiers	LR	SVM (Linear Kernel)	SVM (Quadratic Kernel)	SVM (Cubic Kernel)
The 10 extracted features used in [11]	71%	70%	72%	76%
STFT coefficients	81%	80%	82%	85%

2.5 Conclusion

This chapter presented a new technique that can be used to assist the neurosurgeon during the DBS procedure by providing an objective assessment of the STN location.

Based on the conducted study, a combination of STFT-based features and a Cubic kernel SVM algorithm was suggested as a high-performance approach that can localize STN during surgery.

The results showed that (a) the proposed approach can localize the STN with an accuracy of 85%; (b) it has superior performance over current clinical techniques; and (c) the technique proposed in this study can be used as a cueing tool in the operating room to assist neurosurgeons with STN surgical targeting.

Bibliography

- [1] G. E. Alexander, “Biology of Parkinson’s disease: pathogenesis and pathophysiology of a multisystem neurodegenerative disorder,” *Dialogues in Clinical Neuroscience*, vol. 6, no. 3, p. 259, 2004.
- [2] L. M. De Lau and M. M. Breteler, “Epidemiology of Parkinson’s disease,” *The Lancet Neurology*, vol. 5, no. 6, pp. 525–535, 2006.
- [3] A. L. Benabid, “Deep brain stimulation for Parkinson’s disease,” *Current opinion in Neurobiology*, vol. 13, no. 6, pp. 696–706, 2003.
- [4] M. Okun, M. Tagliati, and e. a. Pourfar, M and, “Management of referred deep brain stimulation failures: A retrospective analysis from 2 movement disorders centers,” *Archives of Neurology*, vol. 62, no. 8, pp. 1250–1255, 2005.
- [5] R. E. Gross, P. Krack, M. C. Rodriguez-Oroz, A. R. Rezai, and A.-L. Benabid, “Electrophysiological mapping for the implantation of deep brain stimulators for Parkinson’s disease and tremor,” *Movement Disorders*, vol. 21, no. S14, 2006.
- [6] F. J. S. Castro, C. Pollo, O. Cuisenaire, J.-G. Villemure, and J.-P. Thiran, “Validation of experts versus atlas-based and automatic registration methods for subthalamic nucleus targeting on MRI,” *International Journal of Computer Assisted Radiology and Surgery*, vol. 1, no. 1, pp. 5–12, 2006.
- [7] C. Pollo, F. Vingerhoets, E. Pralong, J. Ghika, P. Maeder, R. Meuli, J.-P. Thiran, and J.-G. Villemure, “Localization of electrodes in the subthalamic nucleus on magnetic resonance imaging,” *Journal of Neurosurgery*, vol. 106, no. 1, pp. 36–44, 2007.

-
- [8] A. Benazzouz, S. Breit, A. Koudsie, P. Pollak, P. Krack, and A.-L. Benabid, "Intraoperative microrecordings of the subthalamic nucleus in Parkinson's disease," *Movement Disorders*, vol. 17, no. S3, 2002.
- [9] S. Wong, G. Baltuch, J. Jaggi, and S. Danish, "Functional localization and visualization of the subthalamic nucleus from microelectrode recordings acquired during DBS surgery with unsupervised machine learning," *Journal of Neural Engineering*, vol. 6, no. 2, p. 026006, 2009.
- [10] P. Guillen, F. Martinez-de Pison, R. Sanchez, M. Argaez, and L. Velazquez, "Characterization of subcortical structures during deep brain stimulation utilizing support vector machines," in *Engineering in Medicine and Biology Society (EMBC), IEEE*. IEEE, 2011, pp. 7949–7952.
- [11] V. Rajpurohit, S. F. Danish, E. L. Hargreaves, and S. Wong, "Optimizing computational feature sets for subthalamic nucleus localization in DBS surgery with feature selection," *Clinical Neurophysiology*, vol. 126, no. 5, pp. 975–982, 2015.
- [12] E. A. Accolla, J. Dukart, G. Helms, N. Weiskopf, F. Kherif, A. Lutti, R. Chowdhury, S. Hetzer, J.-D. Haynes, A. A. Kühn *et al.*, "Brain tissue properties differentiate between motor and limbic basal ganglia circuits," *Human Brain Mapping*, vol. 35, no. 10, pp. 5083–5092, 2014.
- [13] D. Gabor, "Theory of communication. part 1: The analysis of information," *Journal of the Institution of Electrical Engineers-Part III: Radio and Communication Engineering*, vol. 93, no. 26, pp. 429–441, 1946.
- [14] D. W. Hosmer Jr, S. Lemeshow, and R. X. Sturdivant, *Applied Logistic Regression*. John Wiley & Sons, 2013, vol. 398.
- [15] V. Vapnik, "The support vector method of function estimation," *Nonlinear Modeling: Advanced Black-Box Techniques*, vol. 55, p. 86, 1998.
- [16] C. Cortes and V. Vapnik, "Support vector machine," *Machine Learning*, vol. 20, no. 3, pp. 273–297, 1995.

Chapter 3

Unsupervised Clustering Approach for Localization of STN

3.1 Introduction

Parkinson's disease (PD) is one of the most common neurodegenerative diseases that is caused by loss of dopaminergic neurons in the substantia nigra pars compacta [1]. Movement disorders associated with PD are characterized by tremor, rigidity, postural instability, bradykinesia, and gait issues [2]. Deep Brain Stimulation (DBS) surgery is an effective treatment for advanced PD patients. During DBS surgery, continuous high-frequency electrical current is delivered to the subthalamic nucleus (STN) of the basal ganglia to manage some motor symptoms [3]. The surgical outcomes highly depend on the accuracy of the placement of the electrode inside the STN. Since the STN is a very small region (5-7 mm) of the basal ganglia, accurate placement of the stimulating electrode is a challenging task for the surgical team [4].

A technique to target the STN is the use of preoperative Magnetic Resonance Imaging (MRI) [5]. However, the exact location of the motor region of the STN cannot always be identified accurately using MRI. As a result, intraoperative Micro-Electrode Recording (MER) has been used for localizing the STN.

In general, up to five microelectrodes are inserted through a burr hole in the skull on each side of the brain. The microelectrodes record the electrophysiological activities of the neurons along the insertion trajectory. Typically, MER signals are observed visually by the surgical

team during the operation. Electrophysiological activities vary along the insertion trajectory when the electrode passes through different structures of the brain. This variation is interpreted by the experienced surgical team to localize the STN. The neurosurgeon then determines the border of the STN and selects one of the five electrodes for permanent implantation of the stimulating electrode [5, 6]. Several important criteria are considered by the surgical team to localize STN, such as an increase in the background noise level, spike firing count, and changes in the spike firing patterns. Based on these criteria, neurosurgeons determine the choice of microelectrodes (and their depths) for permanent stimulation [7].

The purpose of this chapter is to design an autonomous algorithm (trained based on a clinical dataset) that can assist neurosurgeons in localizing the STN during DBS surgery. An autonomous STN localization that can provide feedback to a neurosurgeon during the procedure can help to reduce the time during the DBS procedure and can have several clinical benefits. The technique can also be beneficial for enhancing the quality of outcomes by reducing possible placement errors. In Chapter 2, supervised machine learning algorithms were used to build the predictive model which means that the labels acquired from the neurosurgeons were used in training. However, in this chapter, we show that even without using the labels (that mark the STN) provided by a neurosurgeon, the proposed technique is capable of localizing the STN with an accuracy of 80%. For this, we designed a composite unsupervised machine learning algorithm to localize the STN and assist the neurosurgeon in determining the optimal placement of electrodes.

In this part of the study, similar to Chapter 2, instead of using the conventional feature space, we evaluate the performance of short-time Fourier Transformation (STFT) as the tool to populate the feature space for the clustering approach. The STFT-based feature space can be obtained during surgery and does not need any pre- or post- processing information.

In the second step, we initially evaluate the performance of two unsupervised learning methods: K-means clustering and Self Organized Map (SOM) Neural Network, on the dataset that we collected during DBS surgeries from 50 PD patients. We compared the output clusters generated by the above-mentioned two clustering algorithms with the labels provided by an experienced neurosurgeon who has done more than 200 DBS surgeries. The results show that using the STFT-based features, the unsupervised algorithms can detect the signature of STN

and localize it with an accuracy about 75%.

In the third step, a composite approach is evaluated that includes both K-means and SOM clustering as two sequential layers of processing. The first layer is a K means clustering technique which is used to reduce the size of the feature space through locating the sub-centers of the input data (STFT-based feature space). The second layer is an SOM neural network that is used to separate the two main clusters (STN versus outside of STN). We have shown that the proposed composite technique can localize the STN with an accuracy of 80%. It also reduces the training complexity, and therefore the clustering time.

3.2 Methods and Materials

3.2.1 Demographic Data

For this part, we collected and used MER signals from 50 individuals with PD who had previously undergone DBS implantation. The average age was 60 ± 6 yrs (34 male and 16 female). On average, each patient had 10 microelectrodes inserted into their brain. Details of the data acquisition procedure are provided in the next subsection. All the participants had been diagnosed with PD and had begun to lose efficiency of drug treatment. These patients suffered from severe motor fluctuations despite the optimal dosage of medication. These patients were eligible to DBS procedure recording to the requirements determined by the neurosurgical team at London Health Science Center.

Most of the PD patients received bilateral implantations of quadripolar electrodes (Medtronic Inc., Minneapolis, MN, USA) into the subthalamic nucleus of both the left and right cerebral hemispheres during DBS surgery. All these STN-DBS surgeries took place at Western University Hospital in London, Ontario, Canada. The retrospective review was approved by the local Human Subject Research Ethics Board (HSREB) office at the University of Western Ontario (REB # 109045). All participants provided written informed consent before this study participation.

3.2.2 Surgical Procedure and Data Acquisition

All patients discontinued short-acting Parkinson medications 12-hours prior to surgery. Pre-operative MRI was obtained to determine the coordinates of the anterior commissure (AC), posterior commissure (PC) and the STN. An axial T2-weighted image and postgadolinium (Gd) volumetric axial T1-weighted sequence was used for the coordinate localization (Signa, 1.5T, General Electric, Milwaukee, Wis). STN target planning was carried out using the midpoint between the AC and PC points and the standard stereotactic coordinates: 12.0 mm lateral, 2.0 mm posterior and 4.0 mm ventral. The center of the STN was used as the surgical zero-point. Trajectory planning for the microelectrodes was done using the post-Gd volumetric T1-weighted sequence, ensuring avoidance of the ventricles and blood vessels. All surgical planning was done using the StealthStation (StealthStation, Medtronic Corp, MN). A burr-hole was drilled in the skull. The StarDrive (FHC Inc., Bowdoinham, ME) was mounted to the arc at 30.0 mm above the surgical target and five cannulas with stylets were lowered to 10.0 mm above the target. The stylets were then removed from the cannulas and five 60 μm diameter tungsten microelectrodes were inserted into the cannulas with an impedance of 0.5-1.0 $\text{m}\Omega$ at 1kHz (FHC Inc., Bowdoinham, ME). Signals were recorded from 10.0 mm above the preoperatively determined target zero point to well below the ventral (bottom) border of the STN, generally looking for activity indicative of the substantia nigra (4.0 - 5.0 mm below the zero-point). The drive was advanced in 1.0 mm increments and 0.5 mm increments within the target nucleus. At each depth, advancement was paused to allow any artifact to be resolved. Once a clean recording was observed a 10-second recording was collected prior to advancing the electrodes further. The signals were sampled (24kHz, 8 bit), amplified (gain: 10,000) and digitally filtered (bandpass: 500-5000 Hz, notch: 60Hz) using the Leadpoint recording station (Leadpoint 5, Medtronic). A sample MER signal from a right-side anterior trajectory is given in Figure 3.1. As shown in Figure 3.1, some differences in electrophysiological activities can be seen when comparing signals from the inside and outside of the STN.

3.2.3 Feature Extraction: short-time Fourier Transformation

In this study, we calculated the STFT of the electrophysiological signals and use the STFT coefficients as the feature space for the clustering approach. As can be seen in Figure 3.2, an

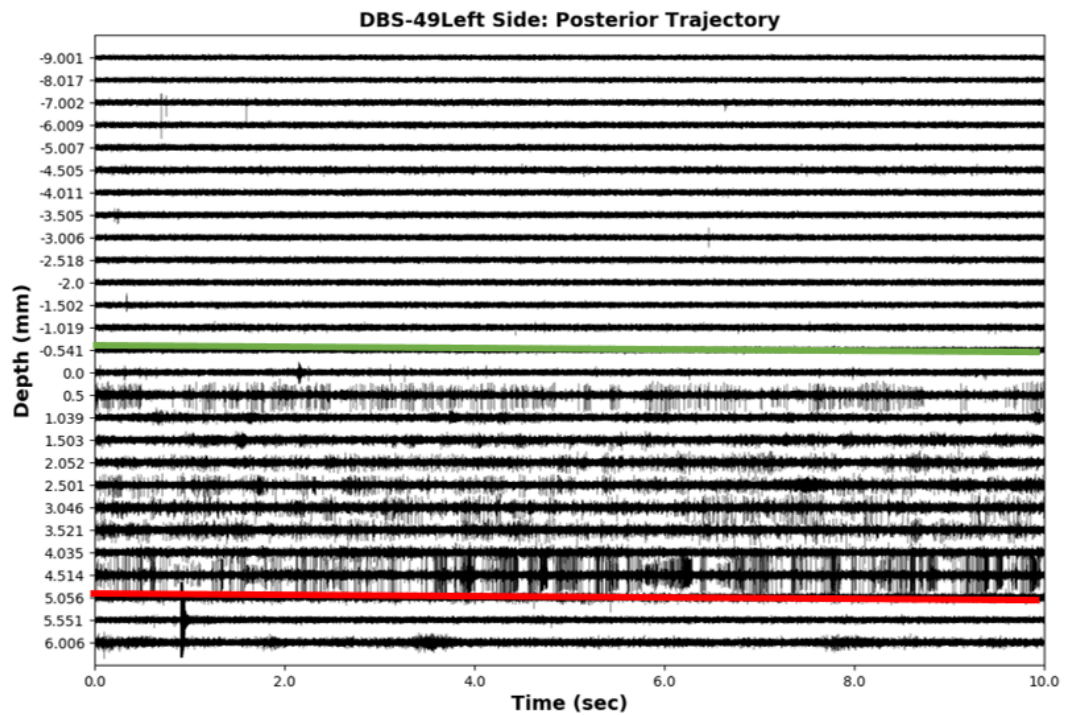


Figure 3.1: MER from an anterior electrode trajectory collected during an STN-DBS case. Negative depth values indicate above the nucleus and positive values indicate below. The green line indicates the dorsal border of STN and the red line indicates the ventral border of STN, as decided by the neurosurgical team.

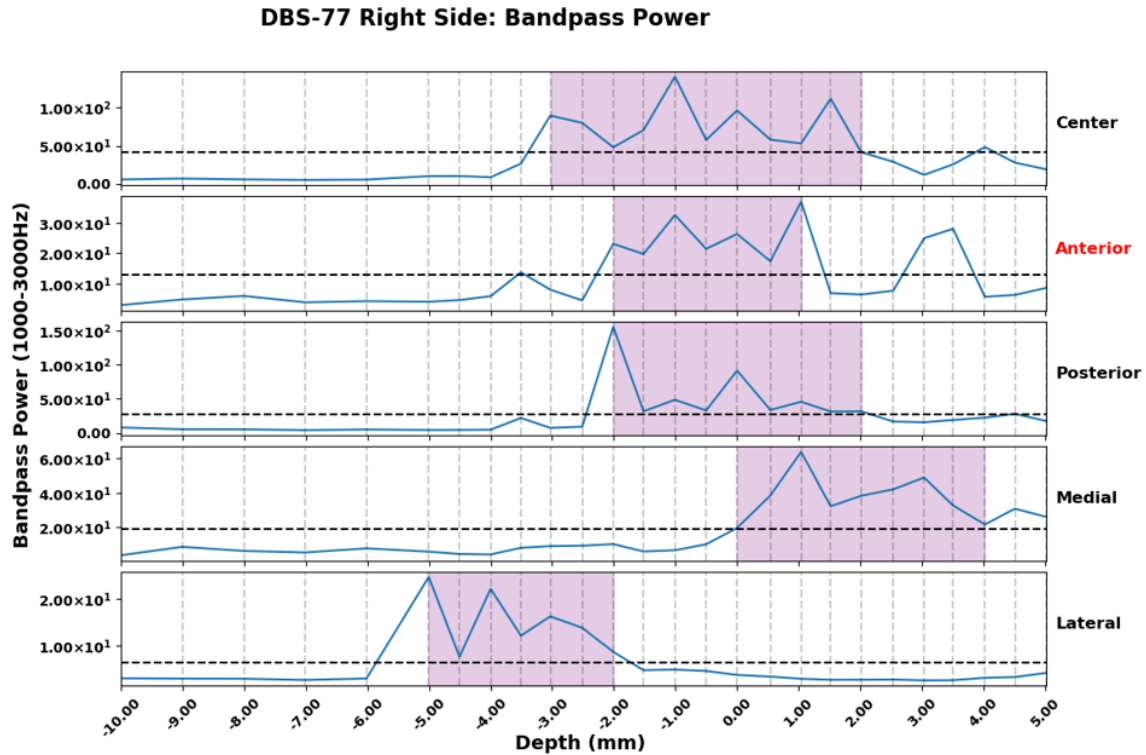


Figure 3.2: The figure shows power from the Short Time Fourier transform (STFT) in the frequency of 1000-3000Hz indicating a single-unit activity. The purple shaded area indicates where the nucleus was determined to be located based on the recordings. Red highlighted depth indicates which channel the surgeon decided to use. Each dotted line represents a recording depth. The power values are discrete and connected with a line for better representation. The negative depth values are above the nucleus and the positive values are below.

increase in the magnitude of the STFT coefficients can be visually observed when the electrode is inside the STN. An STFT-based feature space can provide valuable information about the location of the microelectrodes since they encode the frequency context of the neural activities and the corresponding variation along the insertion path. The STFT-based feature space can be populated during the surgery when the neurosurgeon guides the electrodes toward the target (i.e., the STN). This means that the feature space can be calculated during the operation and no post-operative processing (e.g., spike sorting, normalization along the path) is needed. This is an advantage of the STFT-based feature space in comparison to the ones used in the literature (such as [8], [9]).

3.2.4 Feature Extraction: Conventional Offline Features

As mentioned earlier, the techniques reported in the literature mainly rely on a specific offline feature space designed for the supervised classification of the STN. In this study, to evaluate the performance of the proposed online unsupervised technique in comparison with those in the existing literature, the same feature space is also implemented in addition to the proposed STFT-base feature space.

For this purpose, to populate the offline feature space based on the most effective ten state-of-the-art features reported in [8], [9], and [10] are calculated. The offline features as follows:

- 1) Number of spikes per the 10-second interval;
- 2) Standard deviation of time differences between the spikes of the 10-second interval;
- 3) Pause index: the ratio between the number of spikes greater than 50 ms to the number of spikes less than 50 ms;
- 4) Pause ratio: the ratio between the total time of inter spike intervals greater than 50ms to the total time of those less than 50ms;
- 5) Root Mean Square (RMS) value of the signal amplitude in the 10-second interval;

$$d = \sqrt{\frac{\sum_{i=1}^N x_i^2}{N}}; \quad (3.1)$$

where, each x_i corresponds to a sample in the dataset ($x_i \in X = \{x_1, x_2, \dots, x_n\}$) and N is the number of samples in each signal;

- 6) Spiking rate: number of spikes per unit time.
- 7) Teager Energy, which can be calculated as follows:

$$E = \sum_{i=2}^{N-1} x_i^2 - x_{i-1}x_{i+1}; \quad (3.2)$$

8) Zero crossing: the number of zero crossings in each 10-second interval:

$$k = \frac{1}{2} \sum_{i=1}^{N-1} |sgn(x_{i+1}) - sgn(x_i)|; \quad (3.3)$$

where, function $sgn(x)$ returns 1 for $x > 0$, -1 for $x < 0$, and 0 for $x = 0$.

9) Curve length: the sum of consecutive distances between points in the 10-second interval

$$L = \sum_{i=1}^{N-1} |x_{i+1} - x_i| \quad (3.4)$$

10) Threshold (γ):

$$\gamma = \frac{3}{N-1} \sqrt{\sum_{i=1}^N (x_i - \bar{X})^2} \quad (3.5)$$

where \bar{X} is the average of the 10-second time interval.

It should be noted that the offline feature space reported in [8], [9], [10] requires a specifically designed normalization and standardization process which can only be done post-operatively. As explained in [9], the offline features should be normalized considering the standard deviation of the calculated features in the entire insertion trajectory. Thus, this requires the MER data from the entire trajectory, which is not feasible during online processing of the neural activities. The above-mentioned process is required due to the possibility of instability in feature calculations [8]. This makes the existing approaches post-operative validation techniques which can help to evaluate the quality of the conducted operation. However, it does not allow for STN localization during the operation.

3.3 Classifiers

After extracting features from MER signals, the performance of our clustering algorithms, K-means, SOM Neural Network, and composite K-means-SOM was evaluated in locating the STN. A dataset was collected from 50 PD patients during DBS surgery. The output of our clustering algorithms was compared to the labels provided by a neurosurgeon (with experience of more than 200 DBS surgeries).

3.3.1 K-means

K-means algorithm was first introduced by Macqueen, [11] and is the most popular clustering algorithm. K-means clustering is commonly used to partition signals into k clusters. First, it initializes cluster centers randomly or according to the user's specifications and then iteratively refines the new cluster centers. If the given data set is $X = x_1, \dots, x_N, x_n \in \mathbb{R}^d$ (real number). K-means separates k clusters such that a clustering criterion is optimized. The optimization objective function is as follows:

$$E(m_1, m_2, \dots, m_M) = \sum_{i=1}^N \sum_{k=1}^M I(x_i \in C_k) |x_i - m_k|^2 \quad (3.6)$$

In (3.6), m_1, m_2, \dots, m_M are cluster centers and $I(X) = 1$ if X is true and 0 otherwise. Minimizing this cost function gives the best cluster.

The steps of the K-means clustering algorithm are given below:

- Initialization step
 1. Pick k cluster centers randomly.
 2. Assign each sample to the closest center.
- Iteration step
 1. Compute the means in each cluster.
 2. Re-assign each sample to the closest mean.
- Iterate until the cluster center values stop changing. The number of clusters depends on the problem, and for our data, we set k to two since we want to cluster signals from outside and inside of STN.

3.3.2 Self Organized Map

The SOM is an unsupervised learning neural network method which was presented by Kohonen *et al.* in 1982 [12]. The aim of this network is to give a similarity graph of input data and map it to a low dimensional output space [12]. It also has the capability to cluster similar features in

the input data in different groups. It is a great tool for comprehensive visualization of the data in a lower dimensional space; where the clusters can be clearly identified. The SOM usually has two layers; an input layer and an output layer which are directly connected, which means that each node in the output layer is fully connected to each node in the input layer but the nodes in each layer have no connection to each other [13]. The SOM consists of neurons on a low dimensional grid; usually two dimensional (2-D).

The input of the first layer consists of feature vectors $x_i = [x_{i1}, x_{i2}, \dots, x_{id}] \in R^d$. Each neuron has a dimensional weight vector $w_u = [w_{u1}, w_{u2}, \dots, w_{ud}] \in R^d$. At the beginning of the training, w_u is initialized randomly from the input vector domain. The Euclidean distances from x_i and all w_u are computed. The winning neuron or best match unit (BMU) is the one that has the w_u closest to x_i [14]. Weights of the nodes will update In Figure 3.3, an example of the BMU and winning neurons is shown.

The SOM has been widely used in dimension reduction classification problems. Figure 3.4 shows the Hit Map of the STFT features with two neurons.

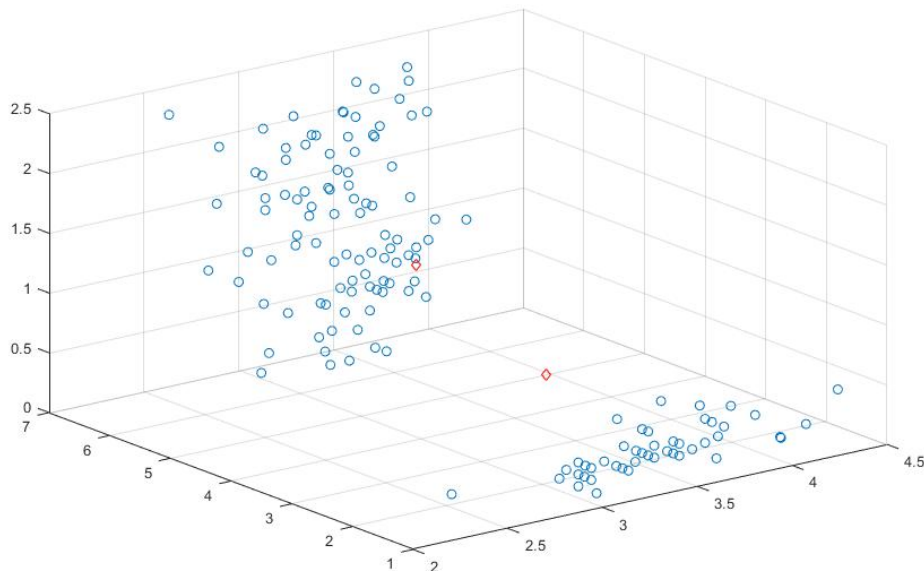


Figure 3.3: An example of the Best Unit Map or winning neurons for the sample data set with two clusters. Blue dots are the example data and red dots are the winning neurons which separated the dataset.

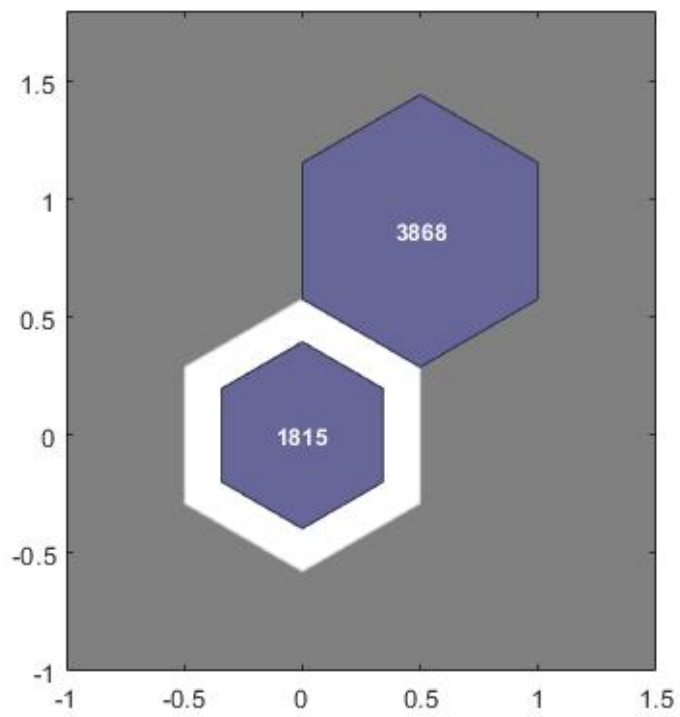


Figure 3.4: Hit Map units of the Self Organized Map with two neurons for STFT features. It shows the two clusters from the data. 3868 signals were labeled as zero and 1815 were labeled as class one.

3.3.3 Composite K-means-SOM

Combinations of K-means and SOM have been commonly used to achieve a better performance than using the individual methods [15]. In this work, we used a composite of K-means and SOM as two layers of processing to increase the clustering accuracy. In the first step, K-means clustering is applied on the signals to reduce the dimension of the feature space. Then, in the second step, the SOM Neural Network is used on the reduced-order feature space to combine and fuse the sub-centers, detect the connections, and form the two main clusters (inside and outside of STN). By using this combination, we achieved a higher accuracy and reduced the training complexity and time.

3.4 Results

In our dataset, we had a ten-second recording from up to 25 depths. On average, each patient had 10 microelectrodes inserted into their brain. The number of signals that we used from 50 patients was 5683. In this study, we have two sets of features (the STFT-based space and the off-line based spaces) and three unsupervised clustering algorithms (K-means, SOM Neural Network, Composite K-means-SOM), and two clusters.

To calculate and evaluate the performance of the proposed composite technique in comparison to the other mentioned approaches [8], [9], we used the labels provided by the neurosurgeon during the operation. The results of this comprehensive comparative study are given in Table 1. As can be seen in the table, using the STFT-based feature space, the K-mean clustering technique was able to localize the STN with an accuracy of 76.7%. However, using the offline feature space results in a significant drop in the accuracy to a range of 58.4%-61.8%. It should be noted that the proposed composite technique, when using the STFT-based feature space, represented the highest accuracy (80%) in comparison to the other approaches. Thus, from the results shown in Table I, the STFT feature space extracted from the MER signals provides rich features for the clustering algorithms and the composite K-means-SOM is a strong unsupervised tool for clustering the STN.

Table 3.1: Accuracy of Unsupervised Clustering Algorithms

Features \ Clustering method	SOM Neural Network	K-means	Composite K-mean-SOM Clustering
10 extracted features	58.4%	61.8%	64%
STFT coefficients	74%	76.7%	80%

3.5 Conclusion

This chapter presented a new technique that can be used to assist neurosurgeons during Deep Brain Stimulation (DBS) procedure by providing online feedback regarding the location of the electrode with respect to the STN. For this purpose, an unsupervised machine learning algorithm was proposed. In this study, we showed that the STFT features extracted from MER signals during DBS surgery can be very informative about the location of electrodes. Based on the results, we showed that we can cluster the signals from inside and outside of STN without requiring any labeling from the neurosurgeon. To validate the performance, we retrospectively extracted MER data from 50 patients with Parkinson’s disease. A total number of 5683 signals were recorded to build the data set. To be able to compare the results, we extracted the most known features used in the literature. We have shown that the proposed unsupervised machine learning method (Composite K-means-SOM) is capable of localizing STN with an accuracy of 80% using STFT features.

Bibliography

- [1] G. E. Alexander, “Biology of Parkinson’s disease: pathogenesis and pathophysiology of a multisystem neurodegenerative disorder,” *Dialogues in Clinical Neuroscience*, vol. 6, no. 3, p. 259, 2004.
- [2] L. M. De Lau and M. M. Breteler, “Epidemiology of Parkinson’s disease,” *The Lancet Neurology*, vol. 5, no. 6, pp. 525–535, 2006.
- [3] A. L. Benabid, “Deep brain stimulation for Parkinson’s disease,” *Current opinion in Neurobiology*, vol. 13, no. 6, pp. 696–706, 2003.
- [4] R. E. Gross, P. Krack, M. C. Rodriguez-Oroz, A. R. Rezai, and A.-L. Benabid, “Electrophysiological mapping for the implantation of deep brain stimulators for Parkinson’s disease and tremor,” *Movement Disorders*, vol. 21, no. S14, 2006.
- [5] F. J. S. Castro, C. Pollo, O. Cuisenaire, J.-G. Villemure, and J.-P. Thiran, “Validation of experts versus atlas-based and automatic registration methods for subthalamic nucleus targeting on MRI,” *International Journal of Computer Assisted Radiology and Surgery*, vol. 1, no. 1, pp. 5–12, 2006.
- [6] C. Pollo, F. Vingerhoets, E. Pralong, J. Ghika, P. Maeder, R. Meuli, J.-P. Thiran, and J.-G. Villemure, “Localization of electrodes in the subthalamic nucleus on magnetic resonance imaging,” *Journal of Neurosurgery*, vol. 106, no. 1, pp. 36–44, 2007.
- [7] A. Benazzouz, S. Breit, A. Koudsie, P. Pollak, P. Krack, and A.-L. Benabid, “Intraoperative microrecordings of the subthalamic nucleus in Parkinson’s disease,” *Movement Disorders*, vol. 17, no. S3, 2002.

-
- [8] S. Wong, G. Baltuch, J. Jaggi, and S. Danish, “Functional localization and visualization of the subthalamic nucleus from microelectrode recordings acquired during DBS surgery with unsupervised machine learning,” *Journal of Neural Engineering*, vol. 6, no. 2, p. 026006, 2009.
- [9] V. Rajpurohit, S. F. Danish, E. L. Hargreaves, and S. Wong, “Optimizing computational feature sets for subthalamic nucleus localization in DBS surgery with feature selection,” *Clinical Neurophysiology*, vol. 126, no. 5, pp. 975–982, 2015.
- [10] P. Guillen, F. Martinez-de Pison, R. Sanchez, M. Argaez, and L. Velazquez, “Characterization of subcortical structures during deep brain stimulation utilizing support vector machines,” in *Engineering in Medicine and Biology Society (EMBC), IEEE*. IEEE, 2011, pp. 7949–7952.
- [11] J. MacQueen *et al.*, “Some methods for classification and analysis of multivariate observations,” in *Proceedings of the fifth Berkeley symposium on mathematical statistics and probability*, vol. 1, no. 14, 1967, pp. 281–297.
- [12] T. Kohonen, “The self-organizing map,” *Neurocomputing*, vol. 21, no. 1-3, pp. 1–6, 1998.
- [13] L. A. Silva and E. Del-Moral-Hernandez, “A SOM combined with knn for classification task,” in *2011 International Joint Conference on Neural Networks*. IEEE, 2011, pp. 2368–2373.
- [14] M.-C. Su and I.-C. Liu, “Application of the self-organizing feature map algorithm in facial image morphing,” *Neural Processing Letters*, vol. 14, no. 1, pp. 35–47, 2001.
- [15] C.-F. Tsai and C. Hung, “Cluster ensembles in collaborative filtering recommendation,” *Applied Soft Computing*, vol. 12, no. 4, pp. 1417–1425, 2012.

Chapter 4

Ensemble of Supervised Classifiers and Deep Neural Network Results on Detecting the STN

4.1 Introduction

Parkinson's disease (PD) is a progressive neurological disease that affects 1% of people over 60 years of age [1, 2]. Motor features of PD result from the death of dopamine neurons in substantia nigra pars compacta of the Basal Ganglia (BG). Oral pharmacotherapy and surgical intervention are both accepted as treatments. Deep Brain Stimulation (DBS) surgery is used especially in those that have advanced PD [3].

During DBS surgery, a permanent electrode is implanted inside the brain to deliver high-frequency electrical pulses to the subthalamic nucleus (STN) [4]. The outcome of DBS surgery is highly dependent on the accurate placement of the electrode inside the STN. Since the STN is a very small (4-7mm) and deep anatomical region, appropriate and accurate implantation of the electrode is a difficult, challenging and time-consuming task that requires a high level of proficiency and expertise. Due to the sensitivity and importance of implantation, significant intraoperative time is spent on localizing the borders of the STN. In fact, sub-optimal positioning of DBS electrodes accounts for 40% of cases of inadequate efficacy of stimulation post operation [5]. In current practice, preoperative Magnetic Resonance Imaging (MRI) is used to

locate the STN according to a visual atlas [6]. However, the exact location of the motor region of the STN cannot be determined from MRI images [7]. Thus, intraoperative Micro Electrode Recordings (MERs) are also used to localize the STN using electrophysiological properties of the brain tissue surrounding the STN and within the STN itself. In a typical DBS surgery, up to five microelectrodes are inserted through a burr hole in the skull. The microelectrodes record the electrophysiological activity along a track as they are sequentially advanced into the brain by the neurosurgeon [8]. Since each part in the brain has its own characteristic neural activity, that of the STN (such as spike firing counts and patterns) can be recognized over the background noise level. As a result, based on monitoring of this electrophysiological activity, the neurosurgeon decides when the microelectrode has entered the STN [6,9].

Chapter 1 gave a complete literature review of previous studies in the topic of STN localization using MER signals. Based on the studies that were mentioned in Chapter 1, the challenge of designing a data-driven model for detecting both the entry and exit borders of STN in an intraoperative manner is an unmet need. The existing problems are: (a) limited data to be used for generation of the model; (b) the need for using offline techniques and normalized features that require critical post-operative manipulation; and (c) limited machine learning power due to the use of classical techniques for the generation of the data-driven physiological model that can represent the borders of STN.

Thus, in this study, we propose to address the challenge through: (a) collection of a rich and unique data-set to be used for evaluating the possibility of reaching high accuracy intraoperatively; (b) using features that can be calculated intraoperatively with no need of critical postoperative normalization; and (c) relying on the power of the collected dataset and using a state-of-the-art strong machine learning algorithm (i.e. deep neural network) to model the nonlinear neurophysiology in order to model the borders of the STN. This study, reports, for the first time, that using data-driven models it is feasible to get an accuracy higher than 90% for localization of STN intraoperatively.

In this chapter, we attempt to improve the output performance by considering the results from Chapter 2 and 3. An ensemble of supervised classifiers that was presented in Chapter 2 is used here to enhance the result. Also, we have enlarged the dataset compared to the previous chapters to achieve a more robust and generalized model. For this purpose, 713 microelectrode

tracks were collected from DBS surgeries of 100 PD patients. To the best of our knowledge, this is the largest dataset collected for this purpose, which allows us to evaluate the possibility of using complex machine learning algorithms for modeling the neurophysiology based on which we can detect the borders of the STN. Currently, such an assessment is performed entirely visually by the clinician looking at the record and listening to the sound of the activity. Such an approach introduces significant subjectivity to the interpretation and can introduce error in localization. An autonomous STN localization tool that can provide objective feedback to neurosurgeons during the procedure would expedite the surgical procedure, improve placement consistency and accuracy.

The proposed learning technique utilizes a sizable database of clinical data collected and labeled in this study by expert neurosurgeons, which ensures its accuracy. In other words, the knowledge of placement locations and the corresponding MER recordings acquired during 100 surgeries is encapsulated in the training algorithm of the proposed technique. When implemented in the OR, the algorithm can reduce subjectivity of STN localization thereby directly having an impact on placement accuracy.

In this study, we evaluated the performance of several classical and modern classification methods for separating the signals that are from inside and outside the STN to detect its border based on electrophysiological activity. Three sets of different features were extracted from MER signals of 100 PD patients who had previously undergone DBS implantation. The first set of features are the conventional feature space which was used in [10, 11]. The second set of features are the short-time Fourier Transformation (STFT) features, and the third are wavelet transformation features. The main advantage of using STFT and wavelet features over conventional features is that they can be extracted intraoperatively since no postoperative step is needed. In [12], Snellings *et al.*, mention that wavelet-driven background levels on STN were significantly higher than other regions and they can be a reliable source of information to identify the border of STN intraoperatively.

Deep neural networks and four classical machine learning algorithms (Support Vector Machine, Logistic Regression, Weighted k -Nearest Neighborhood and Decision Tree) were used for classification. In addition, to improve the accuracy a new design of an ensemble classifier consisting of four machine learning approaches was also applied to classify and predict the

STN border.

The results of the comparative study support the effectiveness of the designed technique in comparison to the existing methods in the literature. We show that the methods proposed in this study not only significantly improve the accuracy of STN localization using MER signals, but they can also be implemented intraoperatively to provide feedback for the surgical team. In this study, an accuracy of 92% was reported for STN border localization using wavelet transformation features and deep neural networks. As a result, the proposed technique has the potential to be used in the operating room for assisting neurosurgeons during DBS surgery to localize the STN.

4.2 Methods and Materials

4.2.1 Demographic Data and Data Acquisition

Microelectrode recordings were retrospectively acquired from 100 individuals with PD (38 female and 62 male), who had undergone DBS implantation. In total, 713 microelectrode tracks were used in this study as most patients received bilateral implantation of their DBS device. The retrospective review was approved by the local Human Subject Research Ethics Board (HSREB) office at the University of Western Ontario (REB # 109045). Prior to the surgery, all patients received T1 and T2 weighted MRI scans for surgical planning (Signa 1.5T, General Electric, Milwaukee, Wis). Target coordinates were calculated by first defining the anterior commissure and posterior commissure. The midline point was then used to plan the STN target; the initial stereotactic coordinates were: 12.0 mm lateral, 2.0 mm posterior and 4.0 mm ventral to the midline. Adjustments were then made according to the anatomy of the patient. All patients withheld their Parkinsonian medications for 12 hours before surgery.

On the day of surgery, the patients received a CT scan with the Leksell frame in place (Elekta Instruments, Sweden). Transferring the preoperative plan to the frame space was carried out by fusion of the stereotactic CT to the preoperative MRIs (StealthStation, Medtronic Corp, MN). The patients were then brought to the operating room, a sterile field was established, and a burr hole was drilled anterior to the coronal suture. A computer-controlled micro-electrode drive was mounted to the Leksell frame (StarDrive, FHC Inc., Bowdoinham, ME),

and 5 cannulas with stylets were lowered to 10.0 mm above the surgically planned target. The stylets were removed and replaced with 5 tungsten microelectrodes (60 μm diameter) with an impedance of 0.5-1.0 $m\Omega$ at 1kHz (FHC Inc., Bowdoinham, ME). Microelectrode signals were then captured from 10.0 mm to 5.0 mm above the target in 1.0 mm steps. From 5.0 mm onwards, a step size of 0.5 mm was used. Once the ventral border of the STN was found the recordings were completed (generally around 4.0 mm to 5.0 mm below the surgical target). The neurosurgeon and electrophysiologist decided on the best microelectrode track, all microelectrodes were removed, and the final therapeutic electrode was introduced down the selected optimal trajectory. In Figure 4.1 the trajectory of microelectrodes inside the brain is shown. At each recording site, data was collected for 10 seconds, which resulted in ~ 25 -30 recordings for each microelectrode. The signals were sampled (24kHz, 8-bit), amplified (gain: 10000) and digitally filtered (bandpass: 500-5000 Hz, notch: 60 Hz) using the Leadpoint recording station (Leadpoint 5, Medtronic). All the computational analyses were conducted using custom scripts in Python and MATLAB. A sample MER signal from a right-side anterior trajectory is shown in Figure 4.2. This figure demonstrates the difference in electrophysiological signal inside and outside the STN.

4.2.2 Feature Extraction

Feature extraction plays an important role in biomedical signal processing. The features should provide meaningful information to the machine learning algorithms and be efficient in the computational step. In this chapter we implemented three different feature extraction methods: (a) conventional post-operative features, (b) fast fourier transformation, and (c) wavelet transformation. A brief explanation of each method is as follows:

Feature Extraction: Conventional Post-Operative Features

To compare the performance of the technique proposed in this study with that of previous studies, we have extracted the most effective ten state-of-the-art features reported in [10], [11], and [15]. A list of these features for one 10-second interval is given below:

- Number of spikes per the 10-second intervals;

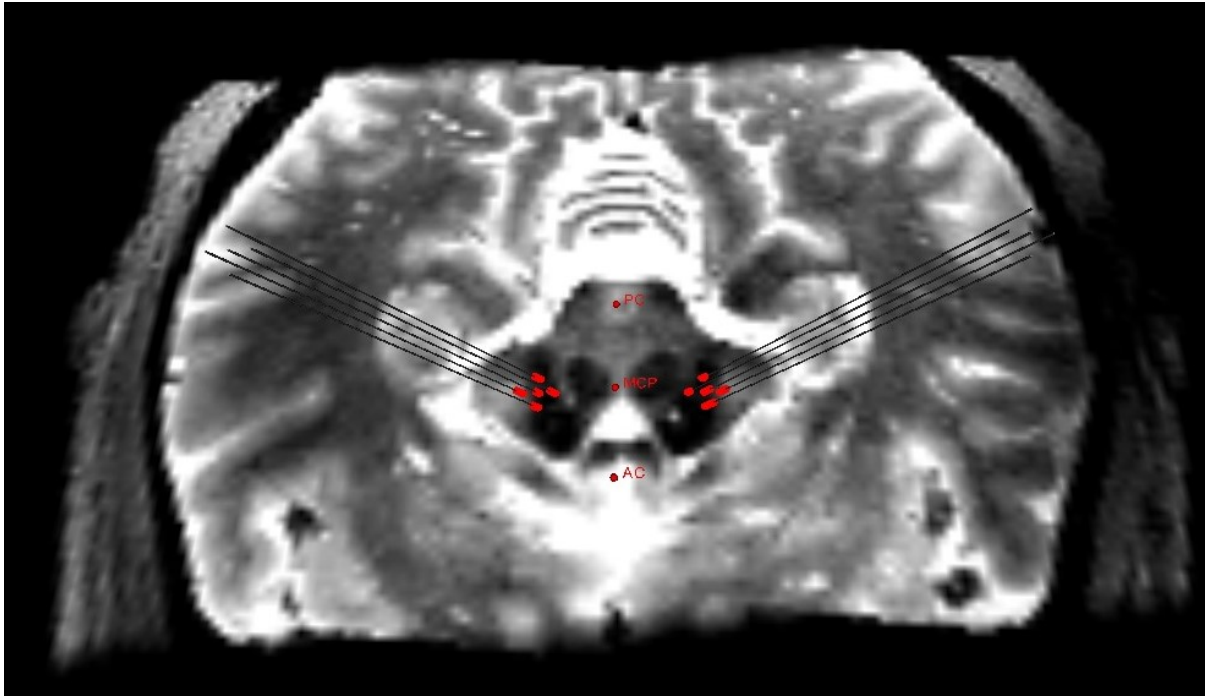


Figure 4.1: Microelectrode trajectory reconstruction. The red lines indicate the depths that the neurosurgeon decided the microelectrodes are inside the STN. The reconstructions and visualizations were performed using custom Python codes, the Visualization Toolkit, and 3D Slicer v4.8 (<https://www.slicer.org>). T2-weighted 7T images were co-registered to the pre-operative CT image containing the Leksell frame. Images were converted to the NIFTI file format using `dcm2niix` [13]. Co-registration was performed using rigid registration tools in `Niftyreg` [14]. The coordinates of the microelectrode trajectories were extracted from `Stealthstation` (Medtronic Corp, MN).

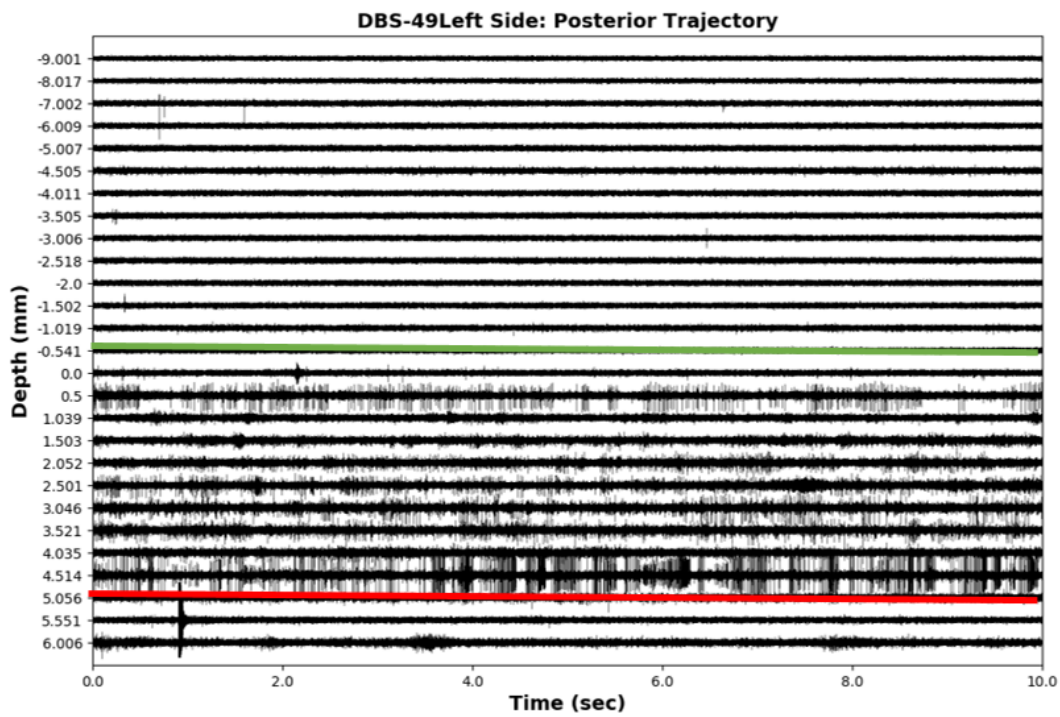


Figure 4.2: MER trace from an anterior microelectrode trajectory from an STN-DBS case at University Hospital, London Health Sciences Center. The microelectrodes were advanced from 10.0 mm to 5.0 mm in 1.0 mm intervals. From 5.0 mm to the end of the trajectory the unit was advanced in 0.5 mm increments. The green line indicates the dorsal border of the STN and the red line indicates the ventral border of the STN, as decided by the neurosurgeon.

- Standard deviation of time differences between the spikes of the 10-second intervals;
- Pause index: the ratio the number of spikes greater than 50 ms to the number of spikes less than 50 ms;
- Pause ratio: the ratio of the total time of inter spike intervals greater than 50ms to the total time of those less than 50ms;
- Root Mean Square (RMS) value of the signal amplitude in the 10-second intervals;
- Spiking rate: number of spikes per unit time (one second).
- Teager Energy, which can be calculated as follows:

$$E = \sum_{i=2}^{N-1} x_i^2 - x_{i-1}x_{i+1}; \quad (4.1)$$

where, $x_i \in X = \{x_1, x_2, \dots, x_n\}$ and N is the number of samples in each signal;

- Zero crossing: the number of zero crossings in each 10-second interval;
- Curve length: the sum of consecutive distances between points in the 10-second interval, as calculated below:

$$L = \sum_{i=1}^{N-1} |x_{i+1} - x_i| \quad (4.2)$$

- Threshold (γ):

$$\gamma = \frac{3}{N-1} \sqrt{\sum_{i=1}^N (x_i - \bar{X})^2} \quad (4.3)$$

where \bar{X} is the average of the 10-second time interval.

As reported in [10], [11], the above-mentioned features need to be normalized because of potential instability in feature calculation. In the normalization procedure, the mean is subtracted from the values of the calculated features and divided by the standard deviation of features in one trajectory. As a result, it is not possible to use these features intraoperatively.

To apply the normalization step, recorded signals from the entire trajectory are required, which is not available while implanting the electrodes. Thus, these features can only be used

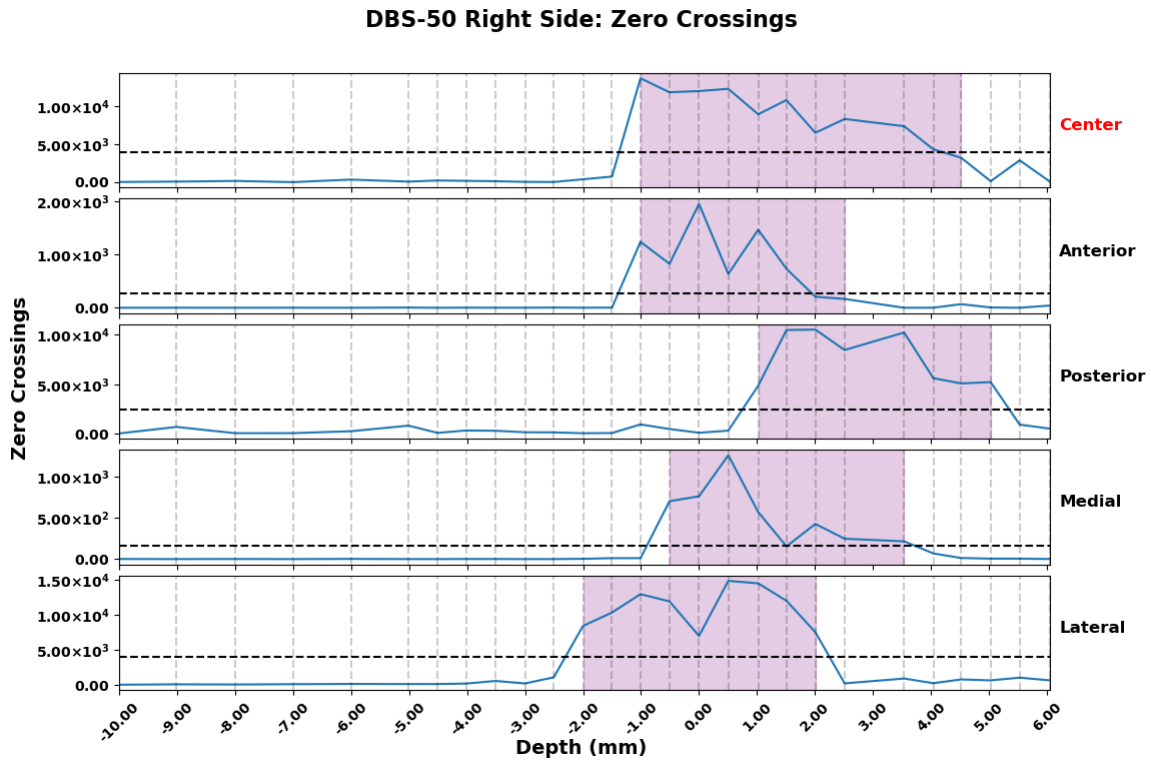


Figure 4.3: The purple shaded area indicates where the nucleus was determined to be based on the recordings. The red highlighted depth indicates which channel the surgeon decided to use. Each dotted line represents a recording depth. Negative depth values are above the nucleus, and positive values are below. The black horizontal dashed line indicates the mean of zero crossing value in each trajectory.

as a postoperative validation method and cannot help to localize the STN during surgery. One of the features, Zero Crossing, is shown in the Figure 4.3 and shows that the difference between the values from inside and outside of the STN nucleus is visible and clear.

Feature Extraction: Fast Fourier Transformation

Fourier Transformation (FT) is one of the methods which can provide valuable information in the frequency domain and is computationally efficient. Frequency data provides information about where the power of signals is concentrated. This is important since it is believed that the frequency content of neuron activities of each structure of the brain is distinctive. Also, since the microelectrode signals from the brain are non-stationary signals and have sudden changes through time, short-time Fourier Transformation (STFT) is selected. STFT applies the Discrete Fourier Transform (DFT) on a fixed-size time window, so frequency and time component of the MER signals can be preserved in the features.

Extracting STFT features from the MER signals can give us meaningful information about the location of the electrode inside the brain. As shown in Figure 4.4, an increase in the power spectral density of DFT is visible when the electrode is inside the STN. It should be noted that by using STFT features, there is no need for the post-normalization step. STFT based features can be used intraoperatively.

As a result, STFT-based feature space can be calculated while recording the MER signals during the operation while the neurosurgeon is implanting the electrodes. This is an advantage of the STFT-based feature space in comparison to the ones used in the literature (such as [10], [11]).

Feature Extraction: discrete Wavelet Transformation

Discrete Wavelet Transformation (DWT), like to the FT, gives the frequency content of the signal and overcomes the drawback of losing time content in DFT. As a result, the extracted wavelet coefficients provide the energy distribution of the signal in time and frequency [16]. Furthermore, there are different types of wavelet mother functions which give us more options

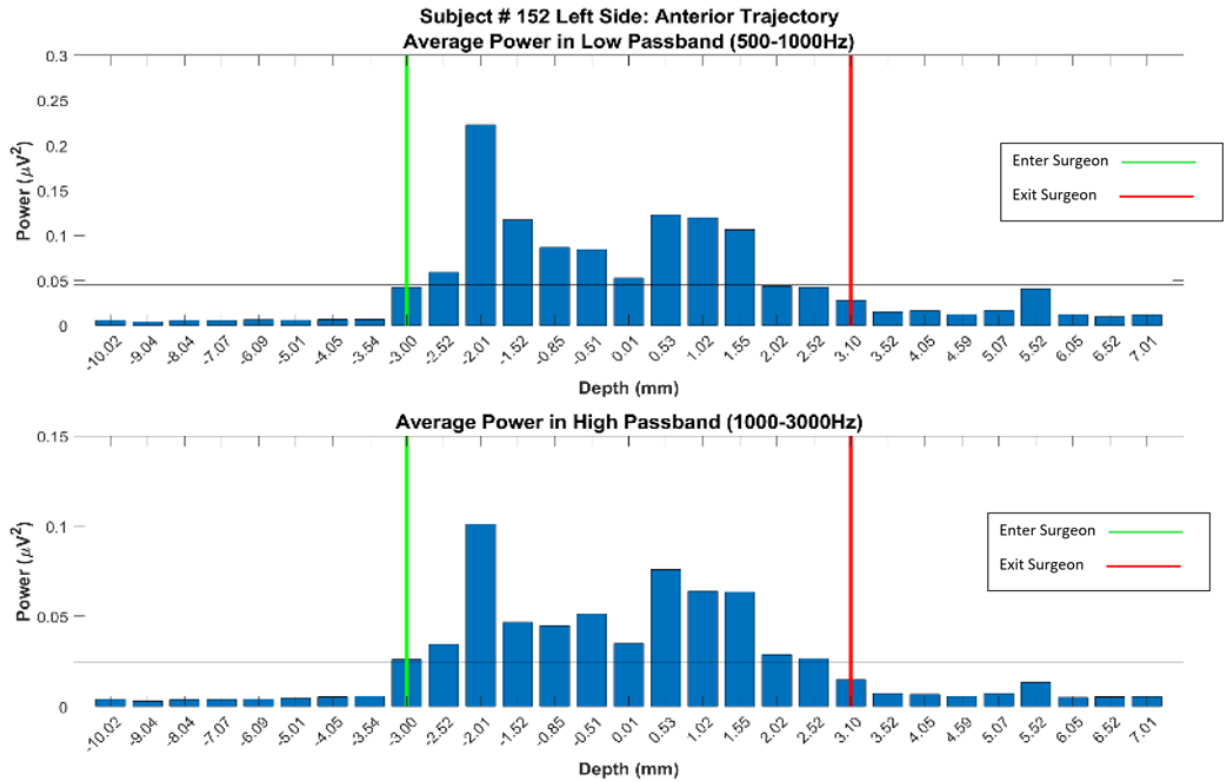


Figure 4.4: Power from DFT in two distinct frequency bands. The upper figure shows the frequency of 500-1000Hz indicating multi-unit activity, and the other figure shows the frequency of 1000-3000Hz indicating single-unit activity. Negative depth values are above the nucleus, and positive values are below. The green line indicates the dorsal border of the STN and the red line indicates the ventral border of the STN, as decided by the neurosurgical team.

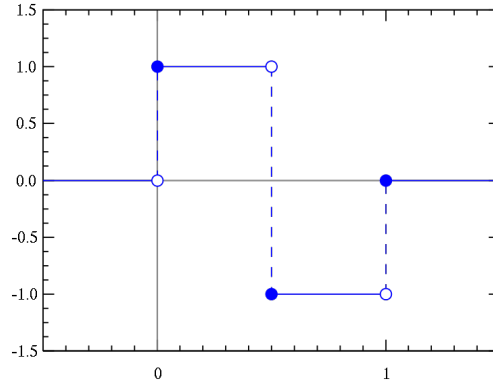


Figure 4.5: The discrete Haar mother Wavelet function.

to extract features from signals. Mathematically, DWT is given by

$$W(u, 2^j) = \sum_{n=-\infty}^{\infty} s(n) \frac{1}{2^{j/2}} \psi\left(\frac{n-u}{2^j}\right) \quad (4.4)$$

where ψ is the mother wavelet (basis function), u represent time and 2^j is the scale parameter for the frequency axis. The signal is down-sampled by 2 to the power level of (2^j) . In our work, Haar wavelet mother functions were used with 4-level decomposition. Haar is a discrete wavelet mother function (shown in Figure 4.5) which is given by

$$\psi(t) = \begin{cases} 1 & 0 \leq t < 1/2, \\ -1 & 1/2 \leq t < 1, \\ 0 & \text{otherwise.} \end{cases}$$

The Haar function is used for analysis of signals with sudden transitions, in this case spikes in the microelectrode signals [17].

4.3 Classifiers

After the feature extraction step, the performance of an ensemble of multiple supervised classifiers and deep neural network was evaluated in locating the STN. The data was collected from 100 PD patients, and the outcome of the classifiers shows the label of the MER signals which is either zero or one. The signals labeled zero indicate that the microelectrode recordings

are from outside of the STN nucleus and those labeled one are recorded from inside the STN. These outcomes were compared with the labels provided by the neurosurgeon (with experience of more than 200 DBS surgeries) for evaluating the accuracy.

4.3.1 The Ensemble of Multiple Classifiers

As an alternative to the modern classifier, in this study, we have evaluated a specific ensemble of conventional classifiers consisting of

1) Support Vector Machine (SVM)

The goal of SVM classifier is to find a hyperplane that can separate the different classes of data. This separation is done by solving an optimization problem and finding the hyperplane which has the largest margin distance of support vectors. Depending on the kernel function of SVM, this separation can be linear or nonlinear with different degrees of nonlinearity and flexibility [18].

Let $x_i \in R, i = 0, 1, \dots, N$ (N is size of the training set) be the input vector and $y_i \in 0, 1$ be the corresponding labels.

$$y(x) = \text{sign}\left(\sum_{i=1}^N \alpha_i y_i \phi(x, x_i) + b\right) \quad (4.5)$$

Where α_i are positive real constants and b is a real constant. $\phi(x, x_i)$ indicates the kernel of the classifier which can be linear or polynomial.

2) Logistic Regression (LR)

LR classifier is especially useful for problems with continuous features and discrete target outputs. The LR model calculates the class membership probability in the data set [19] as shown below.

$$P(1|x, \theta) = \frac{1}{1 + e^{-\theta x}} \quad (4.6)$$

$$P(0|x, \theta) = 1 - P(1|x, \theta)$$

In (4.6), P is the probability of the class, x is the sample signal and θ is determined based on the dataset, usually by maximum-likelihood estimation.

3) Weighted k -Nearest Neighbor (WkNN)

The general idea of k NN classifier is quite simple. It finds the k nearest neighbors of a sample data point x_i . Then it assigns the membership of x based on the distance of it to the k closest neighbors. The Euclidean distance function is typically used in the k NN algorithm. The standard k NN may not work well for imbalanced datasets where the number of examples for some classes are more dominant. For such cases, weighted k NN are more useful which computes the inverse of distance as the weight for each data point. So, the closer points have higher weights than more distant ones.

$$w_i = \frac{1}{d(x_q, x_i)^2} \quad (4.7)$$

Where, w_i is the weight of sample x_i , x_q is the neighbor sample, and $d(x)$ is the distance function. A big advantage of k NN is that it has no cost of training and its weights can be updated online.

4) Decision Tree (DT):

DT uses a sequential approach for assigning labels to the data. There are different types of decision trees such as ID3, C4.5, CART. Most of them work by partitioning the input data along the dimensions which have the most information. In a decision tree, each node represents a feature, the branches are the decision rules, and each leaf represents the label or the target value.

There are some ensemble techniques which construct a multitude of decision trees with a goal to achieve more productivity and overcome the overfitting problem of the DT algorithm. Random forest is one of these ensemble methods which can build multiple DTs by repeatedly re-sampling random subsets of features from input space. Thus, in this study a series of DTs were used by implementing the random forest technique.

- Using the ensemble of these four classifiers can help to enhance the accuracy and better deal with nonlinearity in the data. We also evaluated the performance of each classifier used in the ensemble technique separately.

There are different strategies for combining classifiers. Among the existing techniques,

”majority vote” is a commonly used approach. There are also other combination strategies such as ”boosting” and ”bagging” based on the majority vote method [20]. A weighted majority vote method is used for combining the classifiers here.

Weighted Majority Vote Rule

In the majority vote scheme, the final decision goes with the one that has consensus for it or the one for which more than fifty percent of the individual techniques agree. If each of the classifiers does not give identical classification accuracy, then it is reasonable to attempt to give the more competent classifiers greater weight in making the final decision. This method is called ”weighted majority vote rule” The formula for a weighted majority vote is:

$$y = \underset{i}{\operatorname{argmax}} \sum_{j=1}^m w_j \chi_A(C_j(x) = i), \quad (4.8)$$

where χ_A is the characteristic function $[C_j(x) = i \in A]$, and A is a set of unique class labels. w_j is the weight assigned to classifier j based on its accuracy.

As a result, in this study, we evaluated the performance of an ensemble classifier approach which is based on the weighted majority vote rule and is composed of SVM, LR, $WkNN$, and DT. All results, including the performance of the proposed ensemble technique in addition to the performance of each classifier used in the ensemble technique are given in Section 4.4.

4.3.2 Deep Neural Networks

Artificial Neural Networks (ANNs) have become a popular classifier due to their inherent characteristics such as self-learning, robustness, adaptivity and generalization capability. ANNs are useful especially when there is enough data for training to obtain a good network. They denote a nonlinear mapping between inputs and outputs through multiple layers of neurons that are fully connected to each other. In the training phase, the ANN adjusts to get proper weights and bias to fit the database and produce the desired mapping between inputs and outputs. Processing information is as follows: each neuron in the input layer takes a sample from the dataset, multiplies it by weight, adds a bias value and then passes it to the hidden layer. The hidden layer transforms this data by applying an activation function. In Figure 4.6, a sample of a

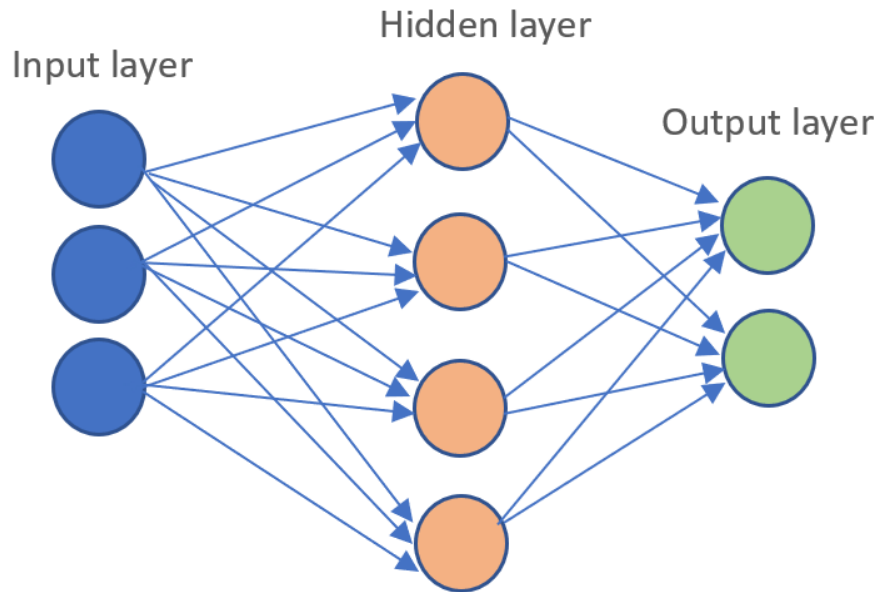


Figure 4.6: A sample of fully connected feedforward neural network with one hidden layer.

neural network with one hidden layer is shown. Here is the mathematical representation:

$$h = f \left(\sum_{p=1}^n W_p^2 f \left(\sum_{q=1}^m W_{pq}^1 X_q + b_p^1 \right) + b^2 \right), \quad (4.9)$$

Where W_{pq} ($q = 1, 2, \dots, m; p = 1, 2, \dots, n$) is the matrix of weights which expresses the weights between a neuron in the input layer and another in the hidden layer, n is the total number of hidden neurons and m is the number of input neurons. Also, X is a vector of values in the input layer, b is the bias and f is the activation function.

A Deep Neural Network (DNN) is a multilayer neural network with several hidden layers capable of discovering unknown feature coherences of input signals. It works best with a large amount of data. There are different parameters for each DNN which need to be chosen for the best performance. In this section, a quick description of these parameters is given.

Deep Learning Parameters

1. Number of hidden layers and the number of nodes in each layer:

Choosing the right number of hidden layers and the number of nodes in each layer is an important step for every type of neural networks as well as DNN. By choosing a higher

number, a more generalized model for the data is achievable but it might lead to some problems like overfitting and overcomplexity of the model. Thus, it is important to select the right numbers for these parameters. Using k-fold cross-validation can be a helpful tool for choosing the proper initial values for these parameters.

2. Regularization and Dropout:

DNNs can be strong classifier models but they have the potential of overfitting due to many hidden layers which also affects their complexity. Therefore, using a regularization method is necessary to avoid or reduce overfitting. Regularization is also called the Weight Decay term since it tries to decrease the magnitude of weights by adding a penalty to the error function. The regularization method that is used in this study is called Ridge Regression or L2.

L2 regression adds the square value of weights to the loss function:

$$L2 = \lambda \sum_i w_i^2, \quad (4.10)$$

where w_i is the weight of a hidden layer and λ is the regularization term. Tuning or finding the right value for λ can avoid the overfitting.

Dropout is also another regularization technique that is used in this study to avoid overfitting. This technique randomly ignores several neurons during training in each layer. In other words, the dropout method disconnects some random nodes from previous and next layers in a neural network. For our problem, a dropout rate of 0.3 was used which means 30% of neurons in every layer were dropped during the training. This method makes the network to be less sensitive to the weights and avoid overfitting the training data. Figure 4.7 shows a simple neural network with two hidden layers before and after applying the dropout.

3. Activation function:

Activation function determines if a neuron is activated or not. It converts the input signal of each node to the output. Various linear and nonlinear activation functions are used for deep learning. In the DNN designed for this problem, the activation functions are Relu

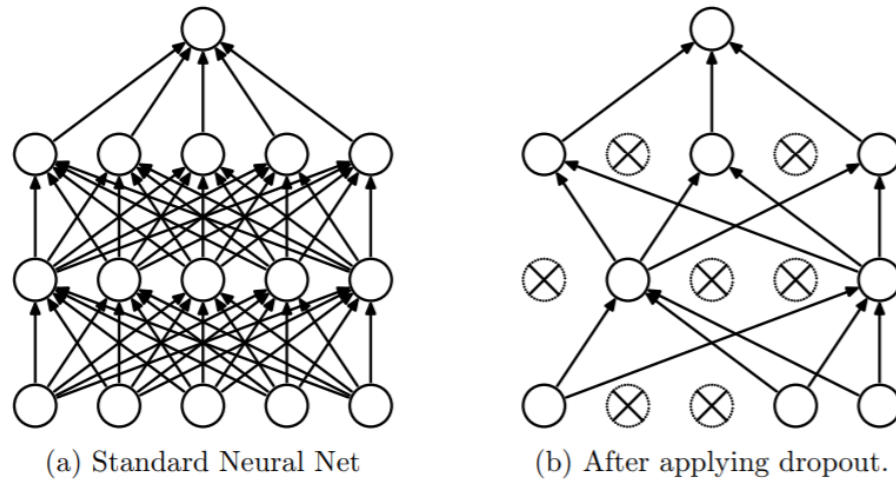


Figure 4.7: Neural Network before and after dropout. (a) is a normal fully connected network. (b) is a network after the dropout. The crossed nodes have been dropped [21].

and Tanh; the formula for these functions is below:

- *Tanh*

$$\tanh(x) = \frac{\sinh(x)}{\cosh(x)} = \frac{1 - e^{-2x}}{1 + e^{-2x}} \quad (4.11)$$

- *Relu*

$$f(x) = \max(0, x) \quad (4.12)$$

These two activation functions were used for the hidden layer nodes. For the output layer, since our problem output is binary, a Sigmoid activation function was used as follows:

- Sigmoid

$$f(x) = \frac{1}{1 + e^{-x}} \quad (4.13)$$

All these activation functions are plotted in Figure 4.8.

4. Loss function and Optimizer

In most networks, training starts with initializing all the weights to a small, random, near zero value at each layer. The objective of training is to update the weights' value and other parameters of the network in order to minimize the cost function. Gradient descent is one way to find the best parameters for the network and it works by updating the parameters in the opposite direction of the derivative of the cost function. In this study, a more efficient version of gradient descent, Stochastic Gradient Descent (SGD)

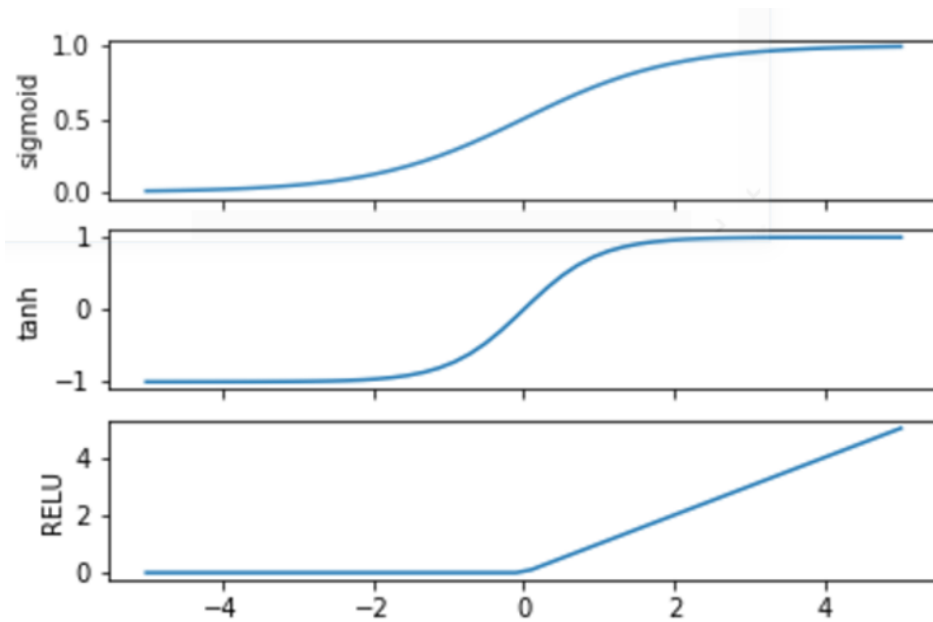


Figure 4.8: Relu, Tanh, and Sigmoid activation functions.

is used. The SGD updates the weights for each sample dataset separately while the with gradient descent all the weights get updated in each iteration. It is important to use a small learning rate when using SGD to reduce the fluctuation in the training since only a single dataset is used in the updating process. The SGD can increase the training speed and it is more efficient than gradient descent because of less computational cost.

RMSprop optimizer is another more efficient way of gradient descent. RMSprop uses the gradient descent with momentum, which makes it converge faster. RMSprop is also used in this study in the training of the DNN model.

In this study, due to the uniqueness and the size of collected data, we have collected over nine thousand microelectrode recordings as ten-second epochs from 100 patients. The DNN was used to model the nonlinear neurophysiology based on which, the STN was localized. To find the most optimal DNN architecture for our problem, several different neural networks were trained and tested. We have chosen the parameters based on the ten-fold cross-validation set. The architecture of the neural network that we chose in this study is a twelve-layer network with ten hidden layers. The number of nodes in each hidden layer was 55 with a dropout rate of 0.3. All these parameters of the chosen DNN were achieved by tracking the accuracy on the test set of ten-fold cross-validation. All the computational analyses were conducted in Python

3.6 (TensorFlow & Keras library).

4.4 Results

The dataset used in this part was enlarged to MER signals from 100 PD patients obtained during DBS surgery. Each recorded MER signal was a ten-second record from each trajectory and depth. On average, up to five microelectrodes were inserted on each side of a patient's brain and in each, trajectory signals were recorded from 25 depths. As a result, the number of signals used in this study was large enough to support the use of a DNN architecture. All three feature sets (conventional postoperative features, STFT-base features, and wavelet features) were extracted from the signals. In the next step, the classifiers (SVM, LR, $WkNN$, DT) were applied to separate the two classes (inside versus outside the STN). As mentioned, a DNN and combination of classical classifiers were used in this study. To calculate and evaluate the performance of the proposed composite technique, the labels provided by the neurosurgeon during the operation were used. The results of this comprehensive comparative study are given in Figure 4.9. As can be seen in the Figure, the ensemble classifier outperforms the single classical classifiers. For example, using STFT-based features, the accuracy of SVM alone is 85%, and this is the highest accuracy among the classical techniques, while using the proposed ensemble of all four classifiers, the accuracy can be improved to 90%.

The best results for this problem were achieved using the wavelet transformation and a DNN. This combination was able to separate the signals intraoperatively in terms of inside and outside the STN with an accuracy of 92%. The confusion matrix for this trained DNN is shown in Table 4.1. The confusion matrix is a tool for performance analysis and it has four cells which report the rates of true positives, true negatives, false positives, and false negatives. In this problem, the false positive rate can be very important since the neurological team would rather be confident that the electrode is inside the STN target than out. By using the presented model (combination of DWT features and DNN classifier), we have achieved a low value of false positive equal to 3%. Also, the precision of this algorithm is calculated as follow:

$$M_{precision}(f) = \frac{TP}{TP + FP}, \quad (4.14)$$

Table 4.1: Confusion Matrix for the DNN Model

		Actual Placement	
		STN	Pre/Post-STN
Predicted Placement	STN	True Positive Rate= 67%	False Positive Rate=3%
	Pre/Post-STN	False Negative Rate=33%	True Negative Rate=97%

and the precision for this model is 95.7% which indicates the robustness of this model.

All the trained algorithms were tested on new test MER signals and this showed that online real-time implementation allows input data to be processed within a short frame of time (less than 1.35 seconds), and provides feedback on location of the electrodes at each depth with respect to the STN. As mentioned before, the major problem with conventional features is that they cannot be used during surgery because they need some postoperative normalization steps. As a result, although these features can provide postoperative validation, they cannot be used during the surgery to localize the STN. However, STFT-based features and wavelet features do not need a post-processing step and can be extracted in real-time during surgery. Thus, from the results shown in Table 4.2, the wavelet feature space extracted from the MER signals provides rich features for the DNN algorithm to assist the neurosurgeon in localizing the STN intraoperatively.

In addition, it is important to note that regardless of the problem with intraoperative implementation of the conventional techniques, they do not have the accuracy of the ones proposed here. In this study, two main approaches were proposed, (a) wavelet feature space used in a DNN, and (b) STFT-based feature space used in an ensemble SVM-LR-*Wk*NN-DT fused using a weighted majority vote. The accuracy of both approaches for localizing the STN was higher than conventional techniques. Unlike conventional techniques [10], [11], both approaches can be implemented intraoperatively with the wavelet-DNN having the highest accuracy.

Thus, from the results shown in Table 4.2, the wavelet feature space extracted from the MER signals provides rich features for a DNN algorithm for assisting neurosurgeons in localizing the STN intraoperatively.

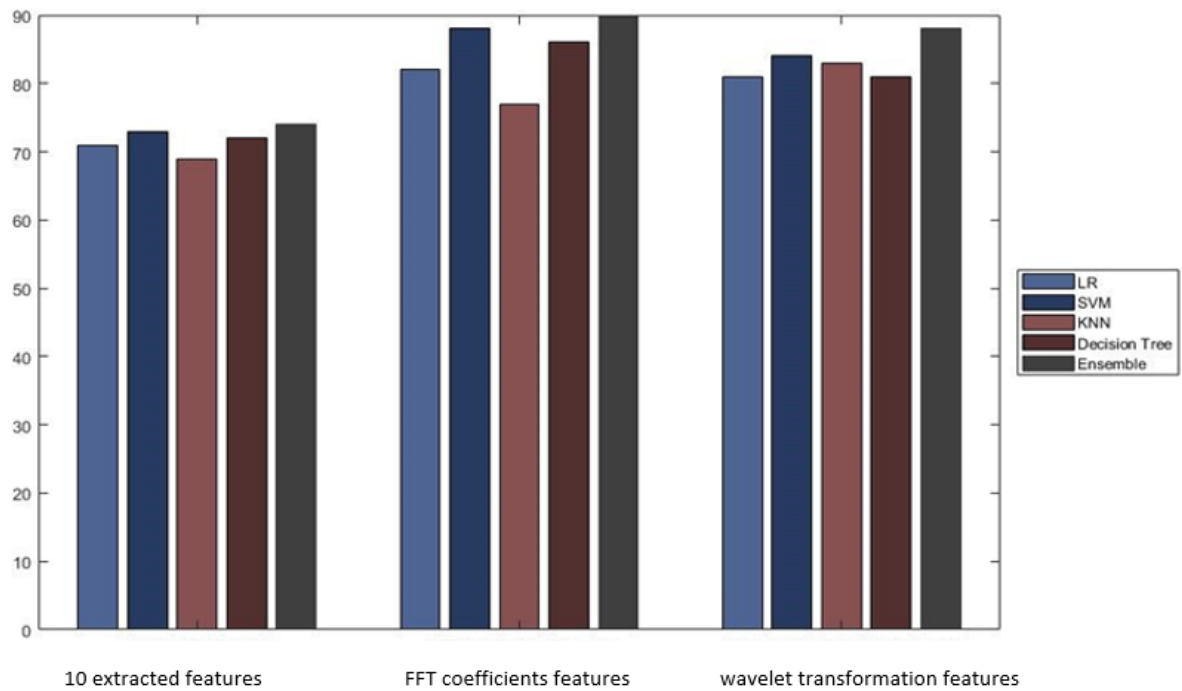


Figure 4.9: Accuracy of Classical Classifiers and Ensemble method for localizing STN.

Table 4.2: Accuracy of Deep Neural Network and Ensemble method

Features\Classifiers	Ensemble of Classical methods	Deep Neural Network
10 extracted features	74%	89%
STFT coefficients	89%	90%
Wavelet Transformation features	88%	92%

4.5 Conclusion

This chapter presented new techniques that can be used to assist the neurosurgeon during DBS surgery by providing accurate localization of the STN. For this purpose, Microelectrode Recording (MER) signals were processed and used in a machine learning algorithm. Based on this study, a combination of discrete wavelet transformation features and a Deep Neural Network algorithm was suggested as a highly accurate approach to localize the STN during DBS surgery with an accuracy of 92%. To validate the performance of this approach, MER data from 100 patients living with Parkinson's disease was used. A total of 9365 signals were recorded to construct the data set. A comparative study was conducted to evaluate the accuracy of the method with that of existing state-of-the-art techniques. The results showed that (a) the proposed approach can localize the STN with an accuracy of 92%; and (b) the technique described in this study can be used as a cueing tool in the operating room to assist neurosurgeons to reach the STN target during DBS surgery in real-time. able

Bibliography

- [1] G. E. Alexander, “Biology of Parkinson’s disease: pathogenesis and pathophysiology of a multisystem neurodegenerative disorder,” *Dialogues in Clinical Neuroscience*, vol. 6, no. 3, p. 259, 2004.
- [2] D. G. Healy, M. Falchi, and e. a. O’Sullivan, “Phenotype, genotype, and worldwide genetic penetrance of LRRK2-associated Parkinson’s disease: a case-control study,” *The Lancet Neurology*, vol. 7, no. 7, pp. 583–590, 2008.
- [3] L. M. De Lau and M. M. Breteler, “Epidemiology of Parkinson’s disease,” *The Lancet Neurology*, vol. 5, no. 6, pp. 525–535, 2006.
- [4] A. L. Benabid, “Deep brain stimulation for Parkinson’s disease,” *Current opinion in Neurobiology*, vol. 13, no. 6, pp. 696–706, 2003.
- [5] M. S. Okun, M. Tagliati, M. Pourfar, H. H. Fernandez, R. L. Rodriguez, R. L. Alterman, and K. D. Foote, “Management of referred deep brain stimulation failures: a retrospective analysis from 2 movement disorders centers,” *Archives of Neurology*, vol. 62, no. 8, pp. 1250–1255, 2005.
- [6] F. J. S. Castro, C. Pollo, O. Cuisenaire, J.-G. Villemure, and J.-P. Thiran, “Validation of experts versus atlas-based and automatic registration methods for subthalamic nucleus targeting on MRI,” *International Journal of Computer Assisted Radiology and Surgery*, vol. 1, no. 1, pp. 5–12, 2006.
- [7] T. Foltynie, L. Zrinzo, and e. a. Martinez-Torres, Irene, “MRI-guided STN DBS in Parkinson’s disease without microelectrode recording: efficacy and safety,” *Journal of Neurology, Neurosurgery & Psychiatry*, p. 2010, 2010.

- [8] J. A. Saint-Cyr and A. Albanese, "STN DBS in PD selection criteria for surgery should include cognitive and psychiatric factors," *Neurology*, vol. 66, no. 12, pp. 1799–1800, 2006.
- [9] C. Pollo, F. Vingerhoets, E. Pralong, J. Ghika, P. Maeder, R. Meuli, J.-P. Thiran, and J.-G. Villemure, "Localization of electrodes in the subthalamic nucleus on magnetic resonance imaging," *Journal of Neurosurgery*, vol. 106, no. 1, pp. 36–44, 2007.
- [10] S. Wong, G. Baltuch, J. Jaggi, and S. Danish, "Functional localization and visualization of the subthalamic nucleus from microelectrode recordings acquired during DBS surgery with unsupervised machine learning," *Journal of Neural Engineering*, vol. 6, no. 2, p. 026006, 2009.
- [11] V. Rajpurohit, S. F. Danish, E. L. Hargreaves, and S. Wong, "Optimizing computational feature sets for subthalamic nucleus localization in DBS surgery with feature selection," *Clinical Neurophysiology*, vol. 126, no. 5, pp. 975–982, 2015.
- [12] A. Snellings, O. Sagher, D. J. Anderson, and J. W. Aldridge, "Identification of the subthalamic nucleus in deep brain stimulation surgery with a novel wavelet-derived measure of neural background activity," *Journal of Neurosurgery*, vol. 111, no. 4, pp. 767–774, 2009.
- [13] X. Li, P. S. Morgan, J. Ashburner, J. Smith, and C. Rorden, "The first step for neuroimaging data analysis: Dicom to nifti conversion," *Journal of Neuroscience Methods*, vol. 264, pp. 47–56, 2016.
- [14] M. Modat, D. M. Cash, P. Daga, G. P. Winston, J. S. Duncan, and S. Ourselin, "Global image registration using a symmetric block-matching approach," *Journal of Medical Imaging*, vol. 1, no. 2, p. 024003, 2014.
- [15] P. Guillen, F. Martinez-de Pison, R. Sanchez, M. Argaez, and L. Velazquez, "Characterization of subcortical structures during deep brain stimulation utilizing support vector machines," in *Engineering in Medicine and Biology Society (EMBC), IEEE*. IEEE, 2011, pp. 7949–7952.

-
- [16] L. M. Bruce, C. H. Koger, and J. Li, “Dimensionality reduction of hyperspectral data using discrete wavelet transform feature extraction,” *IEEE Transactions on Geoscience and Remote Sensing*, vol. 40, no. 10, pp. 2331–2338, 2002.
- [17] J. Rafiee, M. Rafiee, and P. Tse, “Application of mother wavelet functions for automatic gear and bearing fault diagnosis,” *Expert Systems with Applications*, vol. 37, no. 6, pp. 4568–4579, 2010.
- [18] V. Vapnik, “The support vector method of function estimation,” *Nonlinear Modeling: Advanced Black-Box Techniques*, vol. 55, p. 86, 1998.
- [19] D. W. Hosmer Jr, S. Lemeshow, and R. X. Sturdivant, *Applied Logistic Regression*. John Wiley & Sons, 2013, vol. 398.
- [20] J. Kittler, M. Hatef, R. P. Duin, and J. Matas, “On combining classifiers,” *IEEE Transactions on Pattern Analysis and Machine Intelligence*, vol. 20, no. 3, pp. 226–239, 1998.
- [21] N. Srivastava, G. Hinton, A. Krizhevsky, I. Sutskever, and R. Salakhutdinov, “Dropout: a simple way to prevent neural networks from overfitting,” *The Journal of Machine Learning Research*, vol. 15, no. 1, pp. 1929–1958, 2014.

Chapter 5

Concluding Remarks and Future Work

5.1 Concluding Remarks

The goal of this thesis was to design an automated platform for intraoperative localization of the subthalamic nucleus (STN) in deep brain stimulation (DBS) surgery. DBS is a neurosurgical treatment for Parkinson's disease (PD) patients. The main goal of the DBS operation is to implant an electrode inside the STN nucleus to deliver high-frequency electrical current to the motor region of the STN. Implantation can be unilateral or bilateral depending on the severity of PD motor symptoms. In this study, an assistive approach for this localization of the STN target was designed. To this end, the performance of different feature extraction methods and machine learning algorithms was investigated. All these methods were trained and tested on a rich unique dataset collected from DBS surgeries done at University Hospital, London Health Sciences Center, Ontario, Canada.

The platform resulting from this study can be used as a guidance tool during the DBS surgical procedure to show the location of the electrode intraoperatively. This trained learning platform can assist the neurosurgical team to localize the STN nucleus with more accuracy and consistency than is currently possible. Furthermore, the automation of intraoperative electrophysiology analysis reduces the time required for interpretation, which in turn reduces the overall operation time. The next section discusses the contributions in more detail.

5.1.1 Contributions

This thesis introduced and demonstrated different methods for improved localization of the STN nucleus during DBS surgery. The main contributions of the thesis are as follows.

Novel feature extraction methods were presented which allow the method to be used intraoperatively. In the literature, various feature extraction methods have been used; however, most of them cannot be used during surgery since they require post-processing steps. One of these post-processing steps is normalization. In order to normalize the extracted features, all the MER signals from one trajectory are needed. Thus, normalization requires information that is not available in an online manner. In this work, two new feature extraction methods are presented which do not require post-processing. Thus, these features can be extracted and used intraoperatively, which is an important improvement on past methods. In addition, these features can distinguish different firing patterns and signal characteristics of microelectrode recordings. Therefore, the methods can provide valuable input information for the machine learning algorithms.

Also, in this study, different learning algorithms were investigated to automate the process of localization of the STN nucleus. In Chapter 2, the logistic regression algorithm and support vector machine algorithm with various kernel functions were used. In Chapter 3, the performance of some unsupervised machine learning methods was analyzed. The results show that, even without using any labels in the dataset, the STN borders were detectable with high accuracy. This demonstrates the richness of input features in identifying and distinguishing the signal characteristic of microelectrode recording from outside and inside the STN. In Chapter 4, more complex models were investigated such as deep neural networks and an ensemble of four classifiers. Also, a new feature extraction method was presented in this chapter, i.e., wavelet transformation. For this part, the size of the dataset was increased to train the deep learning model. Performance analysis was conducted using the confusion matrix and the highest accuracy was achieved by using wavelet features and deep neural networks.

Overall, the methods that were investigated in this project have shown that the intraoperative automation of STN localization is feasible. The results show that the technique described in this study can be used as a cueing tool in the operating room to assist neurosurgeons to reach

the STN target during DBS surgery in real-time.

In this thesis, the best performance was achieved using the wavelet transformation as the feature extraction tool and implementing a deep neural network as the learning algorithm. This combination can localize the STN with an accuracy of 92%.

5.2 Future Directions

Based on the work described in this thesis, various research directions can be explored to continue this work in the future. The following sections discuss these future directions.

5.2.1 Collecting Intra-operative Data

In DBS surgery, when all the microelectrodes are implanted inside the patient's brain, the neurosurgeon identifies the dorsal and ventral borders of the STN based on the microelectrode recordings. The neurosurgeon will then conduct stimulation testing with each microelectrode, at various currents, to assess patient symptom improvement. The neurosurgeon chooses the best microelectrode based on the patient's responses to these tests. Thus, the patient's responses to the tests have a significant role in the final choice of the microelectrode trajectory to use for DBS electrode implantation. Collecting the stimulation testing data would help to improve the learning algorithm and enrich the dataset for future predictions.

5.2.2 Collecting Post-operative Data

The results of the DBS surgery are highly dependent on the location of the electrode inside the STN. Postoperative follow-up with the patients and looking into their postoperative MRI images can add helpful and important data to this study.

The neurosurgical team cannot be certain about the exact location of the implanted electrode until they perform postoperative imaging and turn the DBS device on. Thus, collecting this postoperative data can help with the learning algorithm input. The trajectory recordings for the electrodes that are not precisely located in the STN can be excluded from the dataset. This will help the machine learning algorithm to learn from the correct input dataset and make accurate future predictions.

5.2.3 Choosing the Best Channel

Finding the exact depth of entry and exit of borders of the STN is an ongoing problem; selecting the most optimally positioned microelectrode is also challenging in DBS surgery. As mentioned in the thesis, up to five microelectrodes are inserted into each side of the patient's brain. These microelectrodes are named based on their anatomical place; central, medial, lateral, anterior, and posterior. At the end of the surgery, one of these five microelectrodes will be chosen for permanent implantation of the DBS electrode.

Therefore, a possible future step would be to add an extension to the learning algorithm in the proposed method which can distinguish different firing patterns on each microelectrode, thereby enabling the choice of the most optimal microelectrode trajectory.

5.2.4 Localization of Globus Pallidus Pars interna (GPi)

Even though both STN and GPi are the potential targets in DBS surgery [1], few studies have been conducted on the localization of the GPi nucleus. Therefore, future research could be carried out to improve the surgical accuracy of GPi DBS targeting. Research is needed to identify the signal characteristics of neurons inside the GPi. Also, implementation of an online automated algorithm for localizing the GPi nucleus is an unmet need.

5.2.5 Models and Hyperparameters

Many different neural network architectures, of varying sizes and parameters have been investigated in this study. However, there is always room for improving the neural network algorithms to be faster and more robust. Techniques such as Bayesian optimization algorithms may identify better models in less time. Moreover, using other types of neural networks such as recurrent neural network and deep belief neural network may help to achieve better results.

Bibliography

- [1] K. R. Wan, T. Maszczyk, A. A. Q. See, J. Dauwels, and N. K. K. King, “A review on microelectrode recording selection of features for machine learning in deep brain stimulation surgery for Parkinson’s disease,” *Clinical Neurophysiology*, 2018.

Chapter 6

Curriculum Vitae

Name: Mahsa Khosravi

Post-Secondary Education and Degrees: AmirKabir University of Technology
Tehran, Iran
2012-2016 B.Sc.
Electrical Engineering (Control Systems)

University of Western Ontario
London, ON
2017 - 2019 M.Sc.
Electrical and Computer Engineering (Robotics and Control)

Related Work Experience: Teaching Assistant
The University of Western Ontario
2017 - 2019

- Control Systems
- Introduction to Mechatronic Design
- Project Management
- Real-Time Embedded Systems

Publications:

• **Mahsa Khosravi**, Seyed Farokh Atashzar, Greydon Gilmore, Mandar S. Jog, and Rajni V. Patel, in "Electrophysiological Signal Processing for Intraoperative Localization of Subthalamic Nucleus during Deep Brain Stimulation Surgery", *IEEE Global Conference on Signal and Information Processing (GlobalSIP)*, 2018 Nov, pp. 424-428, IEEE.

- **Mahsa Khosravi**, Seyed Farokh Atashzar, Greydon Gilmore, Mandar S. Jog, and Rajni V. Patel, in "Unsupervised Clustering of Micro-Electrophysiological Signals for localization of Subthalamic Nucleus during DBS Surgery", *9th International IEEE EMBS Conference on Neural Engineering (NER)*, CA, USA, 2019.
- **Mahsa Khosravi**, Seyed Farokh Atashzar, Greydon Gilmore, Mandar S. Jog, and Rajni V. Patel, "Intraoperative Localization of STN during DBS Surgery using a Data-driven Deep Neural Network Model", submitted to *IEEE Journal of Biomedical and Health Informatics*, 2019.
- **Mahsa Khosravi**, Seyed Farokh Atashzar, Greydon Gilmore, Mandar S. Jog, and Rajni V. Patel, "Online localization of Subthalamic Nucleus during DBS Surgery by using Machine Learning algorithms", Poster presented at: *AGE-WELLS 4th Annual Conference*, BC, CA, 2018.
- **Mahsa Khosravi**, Seyed Farokh Atashzar, Greydon Gilmore, Mandar S. Jog, and Rajni V. Patel, "DBS Electrode Selection in Deep Brain Stimulation Surgery using a Neural Network Model", accepted for presentation at: *41st Engineering in Medicine and Biology Society (EMBC), Annual International Conference of the IEEE*, Berlin, Germany, 2019.